Stabilized scattering matrix formulation for 2D periodic multilayer dielectrics

Andersson, Michael; Sjöberg, Daniel

2025

Document Version:
Publisher's PDF, also known as Version of record

CODEN:LUTEDX/(TEAT-7283)/1-28/(2025)

Stabilized scattering matrix formulation for 2D periodic multilayer dielectrics

Michael Andersson and Daniel Sjöberg

Electromagnetic Theory
Department of Electrical and Information Technology
Lund University
Sweden

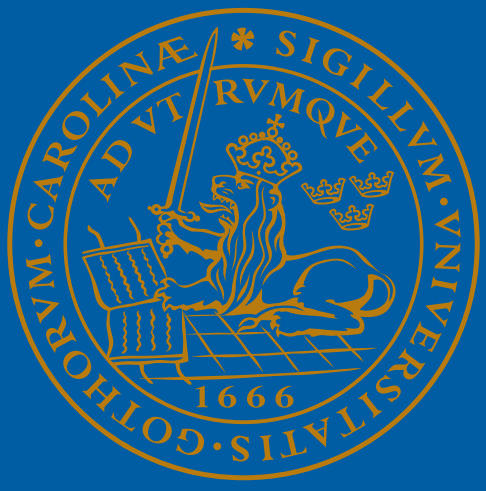

(TEAT-7283)/1-28/(2025): M. Andersson, Stabilization of evanescent wave propagation operators

Michael Andersson
michael.andersson@eit.lth.se

Department of Electrical and Information Technology
Electromagnetic Theory
Lund University
P.O. Box 118
SE-221 00 Lund
Sweden

Editor: Mats Gustafsson

Abstract

This paper proposes an alternative semi-analytical Fourier modal method adapted for general periodic anisotropic gratings made of dielectrics with moderate to low index profiles corresponding to materials ranging from conventional dielectric 3D printing materials to ceramic materials. The proposed method is closely related to classical Rigorous Coupled-Wave Analysis built on scattering matrices, however a key difference is that the new scheme relies on the recently reported concept of stabilized wave propagation operators, leading to improved numerical stability and accuracy for a wider range of structures where *e.g.*, evanescent waves are present. Multilayer structures can be handled in a stable manner using the dissipative property of the Redheffer star product for cascading scattering matrices from which the reflection and transmission of the whole structure is derived. Numerical examples of practical interest as well as importance for future development demonstrate the method's accuracy, efficiency as well as stability through comparison with solutions obtained by finite elements as well as results published in the literature.

1 Introduction

As the demand for high-performance devices grows, 2D periodic multilayer dielectric devices are becoming increasingly crucial in fields like microwave engineering, photonics and radome enclosed sensor applications. Accurately modeling their behavior is essential for designing high performance devices.

Numerical techniques that rely on Fourier expansions of the electromagnetic fields and on grating parameters such as the permittivity and the permeability are in general referred to as Fourier modal methods (FMM) [30]. For example, the Rigorous Coupled-Wave Analysis (RCWA) method introduced in [35] is a well known FMM technique that is commonly used within the optical community. Over the years, researchers have proposed various reformulations of FMM and RCWA to adress specific challenges, such as convergence and numerical stabilization issues. A more extensive survey of the development can be found in [30].

The objective of this paper is on the development and evaluation of an alternative FMM method adapted for the analysis of functional devices built on 1D or 2D periodic multilayer dielectrics. The proposed method is closely related to classical RCWA built on scattering matrices [46, 50, 58]. However, a key difference is that the new scheme relies on the recently reported concept of stabilized wave propagation operators [3] that enhances numerical stability, allowing for the analysis of a broader class of 2D periodic multilayer dielectrics where, *e.g.*, evanescent waves are present. The suggested scheme can handle surface relief gratings made with general anisotropic materials, and multilayer structures are treated in a stable manner using the dissipative property of the Redheffer star product for cascading scattering matrices from which the reflection and transmission of the whole structure are derived [46].

The accommodation of general anisotropic materials prepare future development and generalizations, *e.g.*, in order to adapt the method for more complex grating

geometries. However, the main goal of this study is to evaluate the suitability of using the proposed technique for applications with devices made of periodic multilayer dielectrics having moderate to low index contrast with interest in, *e.g.*, the microwave regime for electrical design of broad band gradient radomes [43]. This paper is limited to consider the alternative FMM formulation without introducing additional techniques such as, *e.g.*, factorization techniques based on the normal vector method or adaptive spatial resolution. The limitation is shown not being severe at least for the considered numerical examples within the paper. A separate section on potential extensions of the proposed method is included in the paper with the aim to introduce suitable techniques for efficiency and accuracy improvements in future development.

The paper is organized as follows. In Section 2 is a detailed presentation of the proposed scheme given and potential extensions are discussed in Section 3. The numerical accuracy, efficiency as well as stability of the new formulation is verified in Section 4 where a number of examples of practical interest as well as importance for future development are given. Finally, the paper is concluded and summarized in Section 5.

2 Stable multimodal scattering matrix formulation

Classical RCWA is adapted for the analysis of periodic functional surfaces, *e.g.*, gratings, where the electromagnetic fields as well as the material parameters are expanded in a plane wave base [31, 35, 36, 37]. The proposed method is closely related to RCWA built on scattering matrices [46, 50, 58]. Similar to RCWA, the proposed formulation is fully vector based, and rigorous in the sense that no approximations are made to Maxwell's equations. The three-dimensional structure is divided into several planar slabs that are invariant in their longitudinal direction as depicted in Figure 1, and owing to the Fourier expansions Maxwell's equations are converted into matrix form in terms of a system of ordinary differential equations (ODE) that model one-dimensional wave propagation.

The Maxwell equations are classically solved in each slab by decomposing into Floquet-Bloch modes, however the propagation of Floquet-Bloch modes is governed by a generalization of the fundamental propagator equation [25, Chapter 10]. The generalization encompasses an extension of the fundamental propagator equation in Fourier space into an infinite system of equations. Through this approach the form of the fundamental equation is kept in order to more easily reformulate the matrix equations into a stable scattering matrix form by using the technique reported in [3]. This section presents in detail the extension of the stabilized scattering matrix formulation into a multimodal form.

The incident wave is assumed being a monochromatic plane wave with harmonic time dependence, and all media are non-conducting and linear, described in general by fully anisotropic tensors. The anisotropic case is mainly of importance for the preparation of future development and generalizations to handle more general settings, *e.g.*, cases with grating geometries that are not aligned with the boundaries of

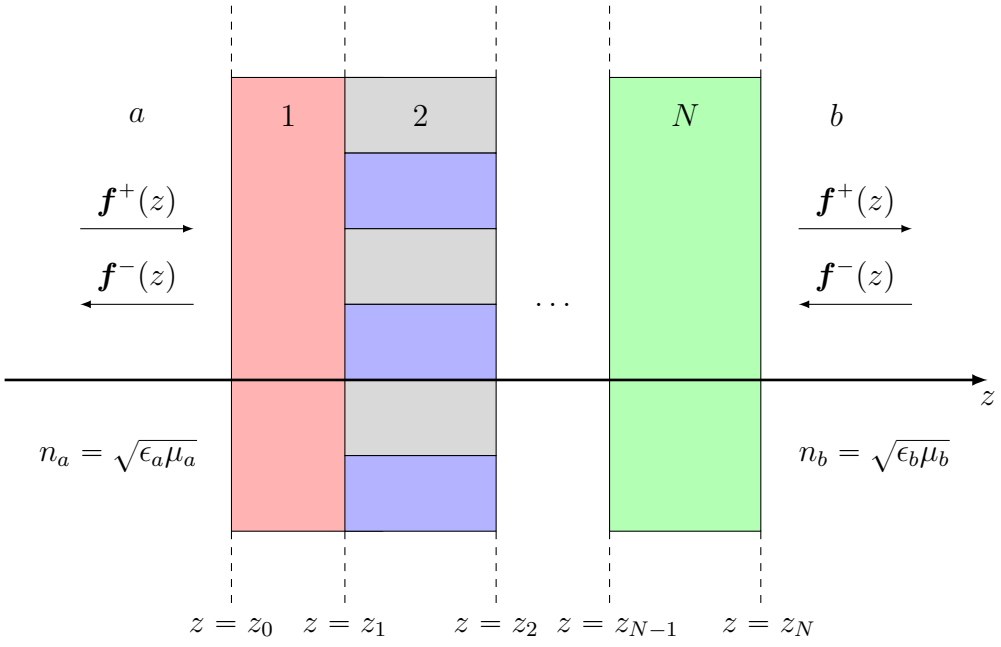

Figure 1: The symbolic representation of the left and right propagating modal split fields $\boldsymbol{f}^{\pm}$ in region a and b, outside the stratified region. Region 2 depicting a slab that is 2D-periodic in the xy plane while invariant in the longitudinal z-direction. The media in regions a and b are arbitrary linear homogeneous and isotropic characterized by refractive index n_a and n_b, respectively.

the reference unit cell, see *e.g.*, [16, 21, 28]. To this end, the scattering matrix form in addition has the advantage that other methods can more easily be incorporated into the general framework of scattering matrices as pointed out in [46].

2.1 Scattering configuration

The scattering configuration of interest is shown in Figure 1, depicting a multi-layer device in terms of a plane-stratified structure where one or several slabs can be 2D-periodic in the xy plane while invariant in the longitudinal z-direction. The analysis of plane-stratified structures is not restricted to time harmonic plane wave incidence since the fields can be decomposed into a spectrum of plane waves, see, *e.g.*, [7, 25]. In this paper the time convention $\mathrm{e}^{-\mathrm{i}\omega t}$ is adopted.

2.2 2D-periodic structures and reciprocal unit vectors

Many functional surfaces can be described by a two-dimensional periodicity, illustrated here by a relative permittivity function $\epsilon(\boldsymbol{r})$ assumed being periodic in the xy plane in accordance with Figure 1 *i.e.*,

$$\epsilon(\boldsymbol{r}) = \epsilon(\boldsymbol{r} + p\boldsymbol{a}_1 + q\boldsymbol{a}_2) \tag{2.1}$$

where $\boldsymbol{a}_1$ and $\boldsymbol{a}_2$ are lattice vectors, whereas p and q are integers, and $\boldsymbol{r} = x\hat{\boldsymbol{x}} + y\hat{\boldsymbol{y}} + z\hat{\boldsymbol{z}}$ is the position vector. The reference cell Ω is spanned by $\boldsymbol{a}_1$ and $\boldsymbol{a}_2$ in the xy plane, and is infinite in the z direction.

Due to the geometry of the reference cell, expansions are most commonly made in terms of the concept of reciprocal unit vectors; see *e.g.*, [48, p.152–153] and the references therein. The reciprocal reference cell Ω' is spanned by the reciprocal unit vectors

$$\boldsymbol{b}_1 = 2\pi \frac{\boldsymbol{a}_2 \times \hat{\boldsymbol{z}}}{\hat{\boldsymbol{z}} \cdot (\boldsymbol{a}_1 \times \boldsymbol{a}_2)} \quad \text{and} \quad \boldsymbol{b}_2 = 2\pi \frac{\hat{\boldsymbol{z}} \times \boldsymbol{a}_1}{\hat{\boldsymbol{z}} \cdot (\boldsymbol{a}_1 \times \boldsymbol{a}_2)} \tag{2.2}$$

We have in general $\boldsymbol{a}_i \cdot \boldsymbol{b}_j = 2\pi\delta_{ij}$, where $\delta_{ii} = 1$ and $\delta_{ij} = 0$ if $i \neq j$. In the simplest case of a quadratic reference cell with period a, we have $\boldsymbol{a}_1 = a\hat{\boldsymbol{x}}$, $\boldsymbol{a}_2 = a\hat{\boldsymbol{y}}$, $\boldsymbol{b}_1 = (2\pi/a)\hat{\boldsymbol{x}}$, and $\boldsymbol{b}_2 = (2\pi/a)\hat{\boldsymbol{y}}$.

2.3 Fourier expansions fields and materials

In analogy with classical RCWA, only Fourier expansion along x and y are utilized, while the z variable remains unchanged. Making use of the *Bloch's theorem* [48, p.153–154], we expand the tangential fields in spatial harmonics according to

$$\begin{cases} \boldsymbol{E}_{\mathrm{t}}(\boldsymbol{r}) = \displaystyle\sum_{p,q} \boldsymbol{s}_{\mathrm{t}}(p,q,z) \mathrm{e}^{\mathrm{i}\boldsymbol{k}_{\mathrm{t}}(p,q)\cdot\boldsymbol{\rho}} \\ \eta_0 \mathbf{J} \cdot \boldsymbol{H}_{\mathrm{t}}(\boldsymbol{r}) = \displaystyle\sum_{p,q} \boldsymbol{u}_{\mathrm{t}}(p,q,z) \mathrm{e}^{\mathrm{i}\boldsymbol{k}_{\mathrm{t}}(p,q)\cdot\boldsymbol{\rho}} \end{cases} \tag{2.3}$$

where $\mathbf{J} = \hat{\boldsymbol{z}} \times \mathbf{I}$ is a rotation in the xy plane by $\pi/2$, $\boldsymbol{\rho} = \hat{\boldsymbol{x}}x + \hat{\boldsymbol{y}}y$ is the lateral position vector, whereas $\boldsymbol{s}_{\mathrm{t}}$ and $\boldsymbol{u}_{\mathrm{t}}$ are vectors formed by the spatial harmonics of the electric and magnetic fields and

$$\boldsymbol{k}_{\mathrm{t}}(p,q) = \boldsymbol{k}_{\mathrm{t}}^{\mathrm{inc}} + \boldsymbol{G}(p,q) = \boldsymbol{k}_{\mathrm{t}}^{\mathrm{inc}} + p\boldsymbol{b}_1 + q\boldsymbol{b}_2 \tag{2.4}$$

where $\boldsymbol{b}_1$ and $\boldsymbol{b}_2$ are the reciprocal basis vectors defined by (2.2). The vector $\boldsymbol{k}_{\mathrm{t}}^{\mathrm{inc}}$ defines the incident transverse wave vector, *i.e.*, the linearly progressing phase of the incident field and the sums in (2.3) are over all integer combinations of the reciprocal lattice vectors $\boldsymbol{b}_1$, and $\boldsymbol{b}_2$. The transverse wave vectors $\boldsymbol{k}_{\mathrm{t}}(p,q) = k_{\mathrm{x}}(p,q)\hat{\boldsymbol{x}} + k_{\mathrm{y}}(p,q)\hat{\boldsymbol{y}}$, are all equal trough the layers of a stacked structure. Corresponding Fourier expansions of the materials *i.e.*, the relative permittivity and permeability tensors $\boldsymbol{\epsilon}$ and $\boldsymbol{\mu}$ are

$$\begin{cases} \boldsymbol{\epsilon}(\boldsymbol{r}) = \displaystyle\sum_{p,q} \boldsymbol{e}(p,q,z) \mathrm{e}^{\mathrm{i}\boldsymbol{G}(p,q)\cdot\boldsymbol{\rho}} \\ \boldsymbol{\mu}(\boldsymbol{r}) = \displaystyle\sum_{p,q} \boldsymbol{m}(p,q,z) \mathrm{e}^{\mathrm{i}\boldsymbol{G}(p,q)\cdot\boldsymbol{\rho}} \end{cases} \tag{2.5}$$

If the structure under consideration has a z-dependent permittivity or permeability distribution, it is common in practice to approximate the material parameters according to the staircase and zigzag approximation, see *e.g.*, [42]. However, more

recently has an alternative technique for the handling of more general cross-sectional shape variations been published, see [60].

The modal wave vectors are decomposed in transverse and longitudinal parts according to

$$\boldsymbol{k}(p,q) = \boldsymbol{k}_{\mathrm{t}}(p,q) + \hat{\boldsymbol{z}} k_{\mathrm{z}}(p,q) \tag{2.6}$$

where $p = -\infty, \ldots, -2, -1, 0, 1, 2, \ldots, \infty$, and $q = -\infty, \ldots, -2, -1, 0, 1, 2, \ldots, \infty$.

The incident medium, is assumed being region a as depicted in Figure 1. Region a is a linear, homogeneous and isotropic medium, characterized by the refractive index $n_a = \sqrt{\epsilon_a \mu_a}$. Furthermore, the incident transverse wave vector components $k_{\mathrm{x}}^{\mathrm{inc}}$ and $k_{\mathrm{x}}^{\mathrm{inc}}$ are defined by

$$\begin{cases} k_{\mathrm{x}}^{\mathrm{inc}} = k_0 n_a \cos\phi \sin\theta \\ k_{\mathrm{y}}^{\mathrm{inc}} = k_0 n_a \sin\phi \sin\theta \end{cases} \tag{2.7}$$

where $k_0 = 2\pi/\lambda_0$ and λ_0 is the wavelength in vacuum. Thus, (2.7) correspond to a three-dimensional tilt of the entire mode set by the incidence angles θ and ϕ in spherical coordinates. Corresponding longitudinal wave numbers $k_{\mathrm{z}}(p,q)$ are given by the dispersion relation

$$k_{\mathrm{z}}(p,q) = (k^2 - k_{\mathrm{t}}(p,q))^{2})^{1/2} = \begin{cases} k_0 \sqrt{n_a^2 - (k_{\mathrm{t}}(p,q)/k_0)^2} & k > k_{\mathrm{t}} \\ \mathrm{i} k_0 \sqrt{(k_{\mathrm{t}}(p,q)/k_0)^2 - n_a^2} & k < k_{\mathrm{t}} \end{cases} \tag{2.8}$$

where $k = k_0 n_a$, and $k_{\mathrm{t}}(p,q) = |\boldsymbol{k}_{\mathrm{t}}(p,q)|$ is the modulus of the transverse wave vectors. By this definition, k_{z} applies to waves traveling in the $+z$-direction and $-k_{\mathrm{z}}$ to waves traveling in the opposite direction.

In numerical computations truncation of the Fourier expansions (2.3) and (2.5), respectively, is inevitable. To this end, the mode indices p and q are truncated in symmetrical intervals according to

$$\begin{cases} p = -P, \ldots, -2, -1, 0, 1, 2, \ldots, P \\ q = -Q, \ldots, -2, -1, 0, 1, 2, \ldots, Q \end{cases} \tag{2.9}$$

and the limits of the resulting symmetrically truncated partial sums are defined by the mode count $M = 2P + 1$ and $N = 2Q + 1$, respectively, for each dimension. Thus, the total number of spatial modes is $L = (4P + 2)(4Q + 2)$, including all modes for both the tangential electric and the magnetic field component expansions *cf.*, (2.3).

2.4 Time harmonic dynamic systems in real space

The generalization of the fundamental equation [25, Chapter 10] into Fourier space starts with the system of partial differential equations describing the dynamics of the tangential time harmonic electromagnetic fields in real space governed by the system of equations

$$\frac{\partial}{\partial z} \begin{pmatrix} \boldsymbol{E}_{\mathrm{t}}(\boldsymbol{r},\omega) \\ \eta_0 \mathbf{J} \boldsymbol{H}_{\mathrm{t}}(\boldsymbol{r},\omega) \end{pmatrix} = \mathrm{i} k_0 \mathbf{M}(\boldsymbol{r},\omega) \begin{pmatrix} \boldsymbol{E}_{\mathrm{t}}(\boldsymbol{r},\omega) \\ \eta_0 \mathbf{J} \boldsymbol{H}_{\mathrm{t}}(\boldsymbol{r},\omega) \end{pmatrix} \tag{2.10}$$

where

$$\mathbf{M}(\boldsymbol{r},\omega) = \begin{pmatrix} \mathbf{M}_1(\boldsymbol{r},\omega) & \mathbf{M}_2(\boldsymbol{r},\omega) \\ \mathbf{M}_3(\boldsymbol{r},\omega) & \mathbf{M}_4(\boldsymbol{r},\omega) \end{pmatrix} \tag{2.11}$$

is a linear map $\mathbf{M}\colon \mathbb{C}^2 \times \mathbb{C}^2 \to \mathbb{C}^2 \times \mathbb{C}^2$ and

$$\boldsymbol{E}_{\mathrm{t}}(\boldsymbol{r},\omega) = \begin{pmatrix} E_{\mathrm{x}}(\boldsymbol{r},\omega) \\ E_{\mathrm{y}}(\boldsymbol{r},\omega) \end{pmatrix}, \quad \mathbf{J} = \begin{pmatrix} 0 & -1 \\ 1 & 0 \end{pmatrix}, \quad \eta_0 \mathbf{J}\boldsymbol{H}_{\mathrm{t}}(\boldsymbol{r},\omega) = \eta_0 \begin{pmatrix} -H_{\mathrm{y}}(\boldsymbol{r},\omega) \\ H_{\mathrm{x}}(\boldsymbol{r},\omega) \end{pmatrix} \tag{2.12}$$

The system (2.10) has the same form as the fundamental equation [25, 44] except that the field quantities in (2.10) have not been Fourier transformed with respect to the lateral coordinates. Anisotropic media is in general described by the relative permittivity and permeability tensors

$$\boldsymbol{\epsilon}(\boldsymbol{r}) = \begin{pmatrix} \epsilon_{\mathrm{xx}} & \epsilon_{\mathrm{xy}} & \epsilon_{\mathrm{xz}} \\ \epsilon_{\mathrm{yx}} & \epsilon_{\mathrm{yy}} & \epsilon_{\mathrm{yz}} \\ \epsilon_{\mathrm{zx}} & \epsilon_{\mathrm{zy}} & \epsilon_{\mathrm{zz}} \end{pmatrix}, \quad \boldsymbol{\mu}(\boldsymbol{r}) = \begin{pmatrix} \mu_{\mathrm{xx}} & \mu_{\mathrm{xy}} & \mu_{\mathrm{xz}} \\ \mu_{\mathrm{yx}} & \mu_{\mathrm{yy}} & \mu_{\mathrm{yz}} \\ \mu_{\mathrm{zx}} & \mu_{\mathrm{zy}} & \mu_{\mathrm{zz}} \end{pmatrix} \tag{2.13}$$

and the blocks of (2.11) are represented by

$$\begin{cases} \mathbf{M}_1(\boldsymbol{r},\omega) = \dfrac{\mathrm{i}}{k_0} \begin{pmatrix} \partial_x(\epsilon_{\mathrm{zz}}^{-1}\epsilon_{\mathrm{zx}}) & \partial_x(\epsilon_{\mathrm{zz}}^{-1}\epsilon_{\mathrm{zy}}) \\ \partial_y(\epsilon_{\mathrm{zz}}^{-1}\epsilon_{\mathrm{zx}}) & \partial_y(\epsilon_{\mathrm{zz}}^{-1}\epsilon_{\mathrm{zy}}) \end{pmatrix} + \dfrac{\mathrm{i}}{k_0} \begin{pmatrix} \mu_{\mathrm{yz}}\mu_{\mathrm{zz}}^{-1}\partial_y & -\mu_{\mathrm{yz}}\mu_{\mathrm{zz}}^{-1}\partial_x \\ -\mu_{\mathrm{xz}}\mu_{\mathrm{zz}}^{-1}\partial_y & \mu_{\mathrm{xz}}\mu_{\mathrm{zz}}^{-1}\partial_x \end{pmatrix} \\ \mathbf{M}_2(\boldsymbol{r},\omega) = -\dfrac{1}{k_0^2} \begin{pmatrix} \partial_x(\epsilon_{\mathrm{zz}}^{-1}\partial_x) & \partial_x(\epsilon_{\mathrm{zz}}^{-1}\partial_y) \\ \partial_y(\epsilon_{\mathrm{zz}}^{-1}\partial_x) & \partial_y(\epsilon_{\mathrm{zz}}^{-1}\partial_y) \end{pmatrix} + \begin{pmatrix} \mu_{\mathrm{yz}}\mu_{\mathrm{zz}}^{-1}\mu_{\mathrm{zy}} - \mu_{\mathrm{yy}} & \mu_{\mathrm{yx}} - \mu_{\mathrm{yz}}\mu_{\mathrm{zz}}^{-1}\mu_{\mathrm{zx}} \\ \mu_{\mathrm{xy}} - \mu_{\mathrm{xz}}\mu_{\mathrm{zz}}^{-1}\mu_{\mathrm{zy}} & \mu_{\mathrm{xz}}\mu_{\mathrm{zz}}^{-1}\mu_{\mathrm{zx}} - \mu_{\mathrm{xx}} \end{pmatrix} \\ \mathbf{M}_3(\boldsymbol{r},\omega) = -\dfrac{1}{k_0^2} \begin{pmatrix} \partial_y(\mu_{\mathrm{zz}}^{-1}\partial_y) & -\partial_y(\mu_{\mathrm{zz}}^{-1}\partial_x) \\ -\partial_x(\mu_{\mathrm{zz}}^{-1}\partial_y) & \partial_x(\mu_{\mathrm{zz}}^{-1}\partial_x) \end{pmatrix} + \begin{pmatrix} \epsilon_{\mathrm{xz}}\epsilon_{\mathrm{zz}}^{-1}\epsilon_{\mathrm{zx}} - \epsilon_{\mathrm{xx}} & \epsilon_{\mathrm{xz}}\epsilon_{\mathrm{zz}}^{-1}\epsilon_{\mathrm{zy}} - \epsilon_{\mathrm{xy}} \\ \epsilon_{\mathrm{yz}}\epsilon_{\mathrm{zz}}^{-1}\epsilon_{\mathrm{zx}} - \epsilon_{\mathrm{yx}} & \epsilon_{\mathrm{yz}}\epsilon_{\mathrm{zz}}^{-1}\epsilon_{\mathrm{zy}} - \epsilon_{\mathrm{yy}} \end{pmatrix} \\ \mathbf{M}_4(\boldsymbol{r},\omega) = \dfrac{\mathrm{i}}{k_0} \begin{pmatrix} \partial_y(\mu_{\mathrm{zz}}^{-1}\mu_{\mathrm{zy}}) & -\partial_y(\mu_{\mathrm{zz}}^{-1}\mu_{\mathrm{zx}}) \\ -\partial_x(\mu_{\mathrm{zz}}^{-1}\mu_{\mathrm{zy}}) & \partial_x(\mu_{\mathrm{zz}}^{-1}\mu_{\mathrm{zx}}) \end{pmatrix} + \dfrac{\mathrm{i}}{k_0} \begin{pmatrix} \epsilon_{\mathrm{xz}}\epsilon_{\mathrm{zz}}^{-1}\partial_x & \epsilon_{\mathrm{xz}}\epsilon_{\mathrm{zz}}^{-1}\partial_y \\ \epsilon_{\mathrm{yz}}\epsilon_{\mathrm{zz}}^{-1}\partial_x & \epsilon_{\mathrm{yz}}\epsilon_{\mathrm{zz}}^{-1}\partial_y \end{pmatrix} \end{cases} \tag{2.14}$$

All material parameters defined by (2.13) are in general functions of spatial position. Notice that lossy materials are described by complex media quantities *i.e.*, $\epsilon_{\mathrm{mn}} = \epsilon'_{\mathrm{mn}} + \mathrm{i}\epsilon''_{\mathrm{mn}}$ and $\mu_{\mathrm{mn}} = \mu'_{\mathrm{mn}} + \mathrm{i}\mu''_{\mathrm{mn}}$, where $m, n = x, y, z$. The derivation of (2.10) is based on decomposition of Maxwell's equations and the field quantities into lateral and longitudinal components relative to the xy-plane following a similar approach as given in [11, p. 10-11]. However, an alternative approach that considers the anisotropic case is reported in *e.g.*, [40, p. 249-256].

2.5 The fundamental equation in discrete Fourier space

The Maxwell equations are classically solved in each slab by expansions of the electromagnetic fields and grating parameters into Floquet-Bloch modes *cf.*, (2.3) and (2.5), respectively. In this paper the general form of the fundamental equation as used in [3] is kept, and by insertion of the field and parameter expansions in the real space dynamical system (2.10) the problem is transformed into discrete Fourier space, *i.e.*, the spatial frequency domain.

After substitution of the Fourier expansions in (2.10) the final form of the matrix equations expressing the fundamental equation in discrete Fourier space is obtained. The result is

$$\frac{\mathrm{d}}{\mathrm{d}z}\begin{pmatrix}\boldsymbol{s}_\mathrm{t}\\ \boldsymbol{u}_\mathrm{t}\end{pmatrix} = \mathrm{i}k_0\mathbf{M}\begin{pmatrix}\boldsymbol{s}_\mathrm{t}\\ \boldsymbol{u}_\mathrm{t}\end{pmatrix} \tag{2.15}$$

with

$$\mathbf{M} = \begin{pmatrix}\mathbf{M}_1 & \mathbf{M}_2\\ \mathbf{M}_3 & \mathbf{M}_4\end{pmatrix}, \quad \begin{pmatrix}\boldsymbol{s}_\mathrm{t}\\ \boldsymbol{u}_\mathrm{t}\end{pmatrix} = \begin{pmatrix}\boldsymbol{s}_\mathrm{x} & \boldsymbol{s}_\mathrm{y} & -\boldsymbol{u}_\mathrm{y} & \boldsymbol{u}_\mathrm{x}\end{pmatrix}^\mathrm{T} \tag{2.16}$$

where $\boldsymbol{s}_\mathrm{t}$ and $\boldsymbol{u}_\mathrm{t}$, respectively are column vectors representing the tangential electric and magnetic amplitude vectors *cf.*, (2.3), whereas the block matrices $\mathbf{M}_1$, $\mathbf{M}_2$, $\mathbf{M}_3$ and $\mathbf{M}_4$ are comprised of the wave vector components and convolution matrices that account for the coupling between electric and magnetic amplitude vectors. In practice the infinite series (2.3) and (2.5) are truncated which limits the number of spatial harmonics and thus, the number of diffraction orders considered in the computation. The matrix $\mathbf{M}$ becomes a linear map $\mathbf{M}\colon \mathbb{C}^{2M}\times\mathbb{C}^{2N}\to\mathbb{C}^{2M}\times\mathbb{C}^{2N}$, where $M = 2P+1$ and $N = 2Q+1$ by truncating the mode index p and q in symmetric intervals according to (2.9), and thus the total number of spatial harmonics is $L = (4P+2)(4Q+2)$. The representations of the blocks $\mathbf{M}_i$, $i = 1,\ldots,4$, are

$$\begin{aligned}\mathbf{M}_1 &= \begin{pmatrix}\mathbf{M}_{11} & \mathbf{M}_{12}\\ \mathbf{M}_{21} & \mathbf{M}_{22}\end{pmatrix}, \qquad \mathbf{M}_2 = \begin{pmatrix}\mathbf{M}_{13} & \mathbf{M}_{14}\\ \mathbf{M}_{23} & \mathbf{M}_{24}\end{pmatrix}\\ \mathbf{M}_3 &= \begin{pmatrix}\mathbf{M}_{31} & \mathbf{M}_{32}\\ \mathbf{M}_{41} & \mathbf{M}_{42}\end{pmatrix}, \qquad \mathbf{M}_4 = \begin{pmatrix}\mathbf{M}_{33} & \mathbf{M}_{34}\\ \mathbf{M}_{43} & \mathbf{M}_{44}\end{pmatrix}\end{aligned} \tag{2.17}$$

where *cf.*, (2.14)

$$\begin{cases}
\mathbf{M}_{11} = -\mathbf{K}_\mathrm{x}[\boldsymbol{\epsilon}_{\mathrm{zz}}*]^{-1}[\boldsymbol{\epsilon}_{\mathrm{zx}}*] - [\boldsymbol{\mu}_{\mathrm{yz}}*][\boldsymbol{\mu}_{\mathrm{zz}}*]^{-1}\mathbf{K}_\mathrm{y}\\
\mathbf{M}_{12} = -\mathbf{K}_\mathrm{x}[\boldsymbol{\epsilon}_{\mathrm{zz}}*]^{-1}[\boldsymbol{\epsilon}_{\mathrm{zy}}*] + [\boldsymbol{\mu}_{\mathrm{yz}}*][\boldsymbol{\mu}_{\mathrm{zz}}*]^{-1}\mathbf{K}_\mathrm{x}\\
\mathbf{M}_{21} = -\mathbf{K}_\mathrm{y}[\boldsymbol{\epsilon}_{\mathrm{zz}}*]^{-1}[\boldsymbol{\epsilon}_{\mathrm{zx}}*] + [\boldsymbol{\mu}_{\mathrm{xz}}*][\boldsymbol{\mu}_{\mathrm{zz}}*]^{-1}\mathbf{K}_\mathrm{y}\\
\mathbf{M}_{22} = -\mathbf{K}_\mathrm{y}[\boldsymbol{\epsilon}_{\mathrm{zz}}*]^{-1}[\boldsymbol{\epsilon}_{\mathrm{zy}}*] - [\boldsymbol{\mu}_{\mathrm{xz}}*][\boldsymbol{\mu}_{\mathrm{zz}}*]^{-1}\mathbf{K}_\mathrm{x}\\
\mathbf{M}_{13} = \mathbf{K}_\mathrm{x}[\boldsymbol{\epsilon}_{\mathrm{zz}}*]^{-1}\mathbf{K}_\mathrm{x} + [\boldsymbol{\mu}_{\mathrm{yz}}*][\boldsymbol{\mu}_{\mathrm{zz}}*]^{-1}[\boldsymbol{\mu}_{\mathrm{zy}}*] - [\boldsymbol{\mu}_{\mathrm{yy}}*]\\
\mathbf{M}_{14} = \mathbf{K}_\mathrm{x}[\boldsymbol{\epsilon}_{\mathrm{zz}}*]^{-1}\mathbf{K}_\mathrm{y} - [\boldsymbol{\mu}_{\mathrm{yz}}*][\boldsymbol{\mu}_{\mathrm{zz}}*]^{-1}[\boldsymbol{\mu}_{\mathrm{zx}}*] + [\boldsymbol{\mu}_{\mathrm{yx}}*]\\
\mathbf{M}_{23} = \mathbf{K}_\mathrm{y}[\boldsymbol{\epsilon}_{\mathrm{zz}}*]^{-1}\mathbf{K}_\mathrm{x} - [\boldsymbol{\mu}_{\mathrm{xz}}*][\boldsymbol{\mu}_{\mathrm{zz}}*]^{-1}[\boldsymbol{\mu}_{\mathrm{zy}}*] + [\boldsymbol{\mu}_{\mathrm{xy}}*]\\
\mathbf{M}_{24} = \mathbf{K}_\mathrm{y}[\boldsymbol{\epsilon}_{\mathrm{zz}}*]^{-1}\mathbf{K}_\mathrm{y} + [\boldsymbol{\mu}_{\mathrm{xz}}*][\boldsymbol{\mu}_{\mathrm{zz}}*]^{-1}[\boldsymbol{\mu}_{\mathrm{zx}}*] - [\boldsymbol{\mu}_{\mathrm{xx}}*]\\
\mathbf{M}_{31} = \mathbf{K}_\mathrm{y}[\boldsymbol{\mu}_{\mathrm{zz}}*]^{-1}\mathbf{K}_\mathrm{y} + [\boldsymbol{\epsilon}_{\mathrm{xz}}*][\boldsymbol{\epsilon}_{\mathrm{zz}}*]^{-1}[\boldsymbol{\epsilon}_{\mathrm{zx}}*] - [\boldsymbol{\epsilon}_{\mathrm{xx}}*]\\
\mathbf{M}_{32} = -\mathbf{K}_\mathrm{y}[\boldsymbol{\mu}_{\mathrm{zz}}*]^{-1}\mathbf{K}_\mathrm{x} + [\boldsymbol{\epsilon}_{\mathrm{xz}}*][\boldsymbol{\epsilon}_{\mathrm{zz}}*]^{-1}[\boldsymbol{\epsilon}_{\mathrm{zy}}*] - [\boldsymbol{\epsilon}_{\mathrm{xy}}*]\\
\mathbf{M}_{41} = -\mathbf{K}_\mathrm{x}[\boldsymbol{\mu}_{\mathrm{zz}}*]^{-1}\mathbf{K}_\mathrm{y} + [\boldsymbol{\epsilon}_{\mathrm{yz}}*][\boldsymbol{\epsilon}_{\mathrm{zz}}*]^{-1}[\boldsymbol{\epsilon}_{\mathrm{zx}}*] - [\boldsymbol{\epsilon}_{\mathrm{yx}}*]\\
\mathbf{M}_{42} = \mathbf{K}_\mathrm{x}[\boldsymbol{\mu}_{\mathrm{zz}}*]^{-1}\mathbf{K}_\mathrm{x} + [\boldsymbol{\epsilon}_{\mathrm{yz}}*][\boldsymbol{\epsilon}_{\mathrm{zz}}*]^{-1}[\boldsymbol{\epsilon}_{\mathrm{zy}}*] - [\boldsymbol{\epsilon}_{\mathrm{yy}}*]\\
\mathbf{M}_{33} = -\mathbf{K}_\mathrm{y}[\boldsymbol{\mu}_{\mathrm{zz}}*]^{-1}[\boldsymbol{\mu}_{\mathrm{zy}}*] - [\boldsymbol{\epsilon}_{\mathrm{xz}}*][\boldsymbol{\epsilon}_{\mathrm{zz}}*]^{-1}\mathbf{K}_\mathrm{x}\\
\mathbf{M}_{34} = \mathbf{K}_\mathrm{y}[\boldsymbol{\mu}_{\mathrm{zz}}*]^{-1}[\boldsymbol{\mu}_{\mathrm{zx}}*] - [\boldsymbol{\epsilon}_{\mathrm{xz}}*][\boldsymbol{\epsilon}_{\mathrm{zz}}*]^{-1}\mathbf{K}_\mathrm{y}\\
\mathbf{M}_{43} = \mathbf{K}_\mathrm{x}[\boldsymbol{\mu}_{\mathrm{zz}}*]^{-1}[\boldsymbol{\mu}_{\mathrm{zy}}*] - [\boldsymbol{\epsilon}_{\mathrm{yz}}*][\boldsymbol{\epsilon}_{\mathrm{zz}}*]^{-1}\mathbf{K}_\mathrm{x}\\
\mathbf{M}_{44} = -\mathbf{K}_\mathrm{x}[\boldsymbol{\mu}_{\mathrm{zz}}*]^{-1}[\boldsymbol{\mu}_{\mathrm{zx}}*] - [\boldsymbol{\epsilon}_{\mathrm{yz}}*][\boldsymbol{\epsilon}_{\mathrm{zz}}*]^{-1}\mathbf{K}_\mathrm{y}
\end{cases} \tag{2.18}$$

In (2.18) the matrices $\mathbf{K}_i$, $i = x, y$ $MN \times MN$, are diagonal matrices of the scaled wave vector components $k_{\mathrm{i}}(p,q)/k_0$, $i = x, y$, whereas $[\boldsymbol{\epsilon}_{ij}*]$ and $[\boldsymbol{\mu}_{ij}*]$, $i, j = x, y, z$ are $MN \times MN$ convolution matrices of all corresponding relative permittivity and permeability Fourier coefficients $e_{ij}(p,q,z)$ and $m_{ij}(p,q,z)$, *cf.*, (2.5). It should be noticed that $[\boldsymbol{\epsilon}_{zz}^{-1}*]$ and $[\boldsymbol{\mu}_{zz}^{-1}*]$ have been replaced with $[\boldsymbol{\epsilon}_{zz}*]^{-1}$ and $[\boldsymbol{\mu}_{zz}*]^{-1}$, respectively in accordance with [39, p. 1777]. Otherwise the appearance of the block matrices of $\mathbf{M}$ in (2.16) in fact resembles the form of corresponding blocks reported in *e.g.*, [45] and [40, p. 256]. Alternative formulations adapted for anisotropic as well as bianisotropic gratings are also found in *e.g.*, [16, 21, 28, 32, 38, 41, 53].

2.6 Some notes related to convergence and truncation

The material properties as well as the electromagnetic fields inside the grating are Fourier expanded in lateral direction and across potential jump discontinuities. At these boundaries the approximated material properties and the fields exhibit complementary jumps, which can lead to numerical artifacts and slow convergence of the method. As shown by [33], the convolution of two functions with concurrent jump discontinuities is one consequence for the slow convergence. In its original formulation FMM provides a very fast convergence for one- and two-dimensional dielectric structures with low to moderate index profile, but owing to the Gibbs phenomenon, *i.e.*, the oscillating behavior of the Floquet-Fourier expansion of discontinuous functions, the convergence is poor for high index contrast profiles, especially for metal–dielectric structures [57]. For additional notes regarding the use of FMM for metals, see [34, p. 2242–2243] and the references therein. For instance, several problems are pointed out in [20] regarding the truncation of the RCWA formulation. To this end, the mathematical justification related to the truncation of the Fourier expansions and the infinite system of differential equations is of great importance, see *e.g.*, [4, 29].

Furthermore, additional techniques necessary for extended applicability of the original formulation are discussed in Section 3. These possible extensions aim to improve efficiency and accuracy in configurations with high index contrast profiles as well as more complex geometries.

2.7 Scattered harmonics in terms of scattering matrix

Scattered spatial harmonic waves as solutions to the fundamental equation (2.15) in Fourier space are sought. To this end, the technique reported in [3] is extended to handle an arbitrary number of spatial harmonics. This means in principle that a multimodal propagator formulation is transformed into corresponding scattering matrix form, from which the ingoing fields connect to the left and right outgoing spatial harmonic waves, *i.e.*, the scattered harmonics.

2.7.1 Modal wave propagation operator

The total tangential electric and magnetic wave modes are all continuous across the interfaces in a planar stratified structure, which implies that the propagator can be extended into a multi-modal setting. Thus, the solution to the modal fundamental equation (2.15) is formally written as

$$\begin{pmatrix} \boldsymbol{s}_{\mathrm{t}}(z) \\ \boldsymbol{u}_{\mathrm{t}}(z) \end{pmatrix} = \mathbf{P}(\boldsymbol{k}_{\mathrm{t}}, z, z_0) \begin{pmatrix} \boldsymbol{s}_{\mathrm{t}}(z_0) \\ \boldsymbol{u}_{\mathrm{t}}(z_0) \end{pmatrix} \tag{2.19}$$

where the propagator $\mathbf{P}$ is a $(4P+2)(4Q+2) \times (4P+2)(4Q+2)$ complex-valued matrix, mapping the tangential electric and magnetic amplitude vectors from z_1 to z.

2.7.2 Modal wave splitting in simple medium

The relative wave impedance operator $\mathbf{Z}_{\mathrm{r}}$ given in [3] can similarly be applied in the modal setting where it relates the electric and magnetic field modes propagating in the $\pm z$-direction within a homogeneous linear isotropic media *i.e.*, *simple media* through

$$\boldsymbol{u}_{\mathrm{t}}(z) = \mp \mathbf{Z}_{\mathrm{r}}(\boldsymbol{k}_{\mathrm{t}})^{-1} \boldsymbol{s}_{\mathrm{t}}(z) \tag{2.20}$$

In analogy with the wave splitting utilized in, *e.g.*, [25, 44] the total tangential electric and magnetic harmonics, $\boldsymbol{s}_{\mathrm{t}}$ and $\boldsymbol{u}_{\mathrm{t}}$, respectively, are related to the set of forward and backward harmonics $\boldsymbol{f}^{\pm}$, propagating in the $\pm z$ directions. Thus, in simple media the relation is given by the modal wave splitting

$$\begin{pmatrix} \boldsymbol{s}_{\mathrm{t}}(z) \\ \boldsymbol{u}_{\mathrm{t}}(z) \end{pmatrix} = \begin{pmatrix} \mathbf{I} & \mathbf{I} \\ -\mathbf{Z}_{\mathrm{r}}^{-1} & \mathbf{Z}_{\mathrm{r}}^{-1} \end{pmatrix} \begin{pmatrix} \boldsymbol{f}^{+}(z) \\ \boldsymbol{f}^{-}(z) \end{pmatrix} \tag{2.21}$$

with inverse

$$\begin{pmatrix} \boldsymbol{f}^{+}(z) \\ \boldsymbol{f}^{-}(z) \end{pmatrix} = \frac{1}{2} \begin{pmatrix} \mathbf{I} & -\mathbf{Z}_{\mathrm{r}} \\ \mathbf{I} & \mathbf{Z}_{\mathrm{r}} \end{pmatrix} \begin{pmatrix} \boldsymbol{s}_{\mathrm{t}}(z) \\ \boldsymbol{u}_{\mathrm{t}}(z) \end{pmatrix} \tag{2.22}$$

The matrices $\mathbf{Z}_{\mathrm{r}}^{-1}$ and $\mathbf{Z}_{\mathrm{r}}$ are given by

$$\mathbf{Z}_{\mathrm{r}}^{-1}(\boldsymbol{k}_{\mathrm{t}}) = \frac{1}{\eta} \left[\begin{pmatrix} \mathbf{K}_{\mathrm{z}}^{-1}\mathbf{K}_{\mathrm{t,x}}^{2} & \mathbf{K}_{\mathrm{z}}^{-1}\mathbf{K}_{\mathrm{t,x}}\mathbf{K}_{\mathrm{t,y}} \\ \mathbf{K}_{\mathrm{z}}^{-1}\mathbf{K}_{\mathrm{t,y}}\mathbf{K}_{\mathrm{t,x}} & \mathbf{K}_{\mathrm{z}}^{-1}\mathbf{K}_{\mathrm{t,y}}^{2} \end{pmatrix} + \begin{pmatrix} \mathbf{K}_{\mathrm{z}}\mathbf{K}_{\mathrm{t,y}}^{2} & -\mathbf{K}_{\mathrm{z}}\mathbf{K}_{\mathrm{t,y}}\mathbf{K}_{\mathrm{t,x}} \\ -\mathbf{K}_{\mathrm{z}}\mathbf{K}_{\mathrm{t,x}}\mathbf{K}_{\mathrm{t,y}} & \mathbf{K}_{\mathrm{z}}\mathbf{K}_{\mathrm{t,x}}^{2} \end{pmatrix} \right] \tag{2.23}$$

and

$$\mathbf{Z}_{\mathrm{r}}(\boldsymbol{k}_{\mathrm{t}}) = \eta \left[\begin{pmatrix} \mathbf{K}_{\mathrm{z}}\mathbf{K}_{\mathrm{t,x}}^{2} & \mathbf{K}_{\mathrm{z}}\mathbf{K}_{\mathrm{t,x}}\mathbf{K}_{\mathrm{t,y}} \\ \mathbf{K}_{\mathrm{z}}\mathbf{K}_{\mathrm{t,y}}\mathbf{K}_{\mathrm{t,x}} & \mathbf{K}_{\mathrm{z}}\mathbf{K}_{\mathrm{t,y}}^{2} \end{pmatrix} + \begin{pmatrix} \mathbf{K}_{\mathrm{z}}^{-1}\mathbf{K}_{\mathrm{t,y}}^{2} & -\mathbf{K}_{\mathrm{z}}^{-1}\mathbf{K}_{\mathrm{t,y}}\mathbf{K}_{\mathrm{t,x}} \\ -\mathbf{K}_{\mathrm{z}}^{-1}\mathbf{K}_{\mathrm{t,x}}\mathbf{K}_{\mathrm{t,y}} & \mathbf{K}_{\mathrm{z}}^{-1}\mathbf{K}_{\mathrm{t,x}}^{2} \end{pmatrix} \right] \tag{2.24}$$

where $\eta = \sqrt{\mu/\epsilon}$, and $k = k_0 n$ are the relative wave impedance and wavenumber, respectively, whereas

$$\mathbf{K}_{\mathrm{t},i} = \mathrm{diag}\left(\frac{k_{\mathrm{t,i}}(p,q)}{|\boldsymbol{k}_{\mathrm{t}}(p,q)|}\right), \quad i = x, y \tag{2.25}$$

and $\mathbf{K}_{\mathrm{z}} = \mathrm{diag}(k_{\mathrm{z}}(p,q)/k)$, $\mathbf{K}_{\mathrm{z}}^{-1} = \mathrm{diag}(k/k_{\mathrm{z}}(p,q))$. The longitudinal wave numbers $k_{\mathrm{z}}(p,q)$ are defined by (2.8).

2.7.3 The multimodal scattering matrix form

Combining (2.19) and the wave splitting relations (2.21) and (2.22) for an arbitrary material a on the left and material b on the right, gives the scattering relation

$$\begin{pmatrix} \boldsymbol{f}^+(z_N) \\ \boldsymbol{f}^-(z_N) \end{pmatrix} = \mathbf{W} \begin{pmatrix} \boldsymbol{f}^+(z_0) \\ \boldsymbol{f}^-(z_0) \end{pmatrix} \tag{2.26}$$

where

$$\mathbf{W} = \begin{pmatrix} \mathbf{W}_{11} & \mathbf{W}_{12} \\ \mathbf{W}_{21} & \mathbf{W}_{22} \end{pmatrix} = \frac{1}{2} \begin{pmatrix} \mathbf{I} & -\mathbf{Z}_{\mathrm{r,b}} \\ \mathbf{I} & \mathbf{Z}_{\mathrm{r,b}} \end{pmatrix} \begin{pmatrix} \mathbf{P}_{11} & \mathbf{P}_{12} \\ \mathbf{P}_{21} & \mathbf{P}_{22} \end{pmatrix} \begin{pmatrix} \mathbf{I} & \mathbf{I} \\ -\mathbf{Z}_{\mathrm{r,a}}^{-1} & \mathbf{Z}_{\mathrm{r,a}}^{-1} \end{pmatrix} \tag{2.27}$$

In order to easily identify the left- and right-going scattered spatial harmonics in terms of the incoming wave fields, one can conveniently reformulate the relation (2.26) into a scattering matrix form defined by

$$\begin{pmatrix} \boldsymbol{f}^-(z_0) \\ \boldsymbol{f}^+(z_N) \end{pmatrix} = \mathbf{S} \begin{pmatrix} \boldsymbol{f}^+(z_0) \\ \boldsymbol{f}^-(z_N) \end{pmatrix} \tag{2.28}$$

However, (2.26) is not necessarily numerically stable when evanescent waves are present which implies the need to reformulate (2.28) into a well-conditioned form [3].

2.8 Stable multimodal scattering matrix form

Evanescent wave fields are in general present in the scattering problems of periodic devices, which implies the need for having a numerically stable formulation [8, 10, 58]. A scheme that utilizes the spectral decomposition of the propagator for the separation of exponentially growing and decaying terms was developed in [3] in order to obtain a well-conditioned formulation. This section revisits the technique used in [3] from which the stable generalized multimodal scattering matrix is found.

2.8.1 Spectral decomposition

The fundamental matrix $\mathbf{M}$ has eigenvectors and eigenvalues $\{\boldsymbol{v}_m, n_m\}$

$$\mathbf{M} \cdot \boldsymbol{v}_m = n_m \boldsymbol{v}_m \tag{2.29}$$

where the eigenvalues n_m are the refractive indices of the propagating modes, which have polarizations given by the eigenvectors $\boldsymbol{v}_m$. The propagator has the same eigenvectors and propagation factors as eigenvalues

$$\mathbf{P} \cdot \boldsymbol{v}_m = \mathrm{e}^{\mathrm{i}k_0 d n_m} \boldsymbol{v}_m \tag{2.30}$$

where d is the thickness of the slab, and the quantity dn_m is often referred to as the optical thickness.

According to the technique reported in [3], we use the left eigenvectors $\boldsymbol{u}_m$ defined by $\boldsymbol{u}_m^* \cdot \mathbf{P} = \mathrm{e}^{\mathrm{i}k_0 dn_m} \boldsymbol{u}_m^*$ rather than the right eigenvectors $\boldsymbol{v}_m$. Spectral decomposition of $\mathbf{P}$, yields

$$\mathbf{U}^\dagger \cdot \mathbf{P} = \mathbf{D} \cdot \mathbf{U}^\dagger \tag{2.31}$$

where $\mathbf{U}$ is a matrix having the left eigenvectors as columns, and $\dagger$ denotes the Hermitian transpose, and $\mathbf{D}$ is a diagonal matrix containing the eigenvalues

$$\mathbf{D} = \begin{pmatrix} \mathrm{e}^{\mathrm{i}k_0 dn_1} & 0 & \dots & 0 \\ 0 & \mathrm{e}^{\mathrm{i}k_0 dn_2} & \dots & 0 \\ \vdots & \vdots & \dots & \vdots \\ 0 & 0 & \dots & \mathrm{e}^{\mathrm{i}k_0 dn_n} \end{pmatrix} \tag{2.32}$$

More details on spectral decomposition of the propagator $\mathbf{P}$ can be found in [25, pp. 663–669]. Note that the eigenvectors $\mathbf{U}^\dagger$ and eigenvalues n_m are computed from the eigenproblem (2.29) for $\mathbf{M}$, and $\mathbf{P}$ is never explicitly computed.

2.8.2 Well-conditioned multimodal scattering matrix form

This section considers a straightforward generalization into multimodal form of the unconditionally stable scattering matrix formulation recently reported [3]. A similar technique that reformulates a transfer matrix approach into a numerically stable scattering matrix formulation has been reported in [11, pp. 4–5].

Accordingly, the scattering matrix form (2.28) is derived through reformulation of the modal wave scattering relation (2.26) for a structure, enclosed by two homogeneous isotropic half-spaces a and b as depicted in Figure 1. The reformulated relation reads

$$\begin{pmatrix} \mathbf{I} & \mathbf{I} \\ -\mathbf{Z}_{\mathrm{r,b}}^{-1} & \mathbf{Z}_{\mathrm{r,b}}^{-1} \end{pmatrix} \begin{pmatrix} \boldsymbol{f}_{\mathrm{b}}^{+} \\ \boldsymbol{f}_{\mathrm{b}}^{-} \end{pmatrix} = \mathbf{P} \begin{pmatrix} \mathbf{I} & \mathbf{I} \\ -\mathbf{Z}_{\mathrm{r,a}}^{-1} & \mathbf{Z}_{\mathrm{r,a}}^{-1} \end{pmatrix} \begin{pmatrix} \boldsymbol{f}_{\mathrm{a}}^{+} \\ \boldsymbol{f}_{\mathrm{a}}^{-} \end{pmatrix} \tag{2.33}$$

where $\mathbf{Z}_{\mathrm{r,a}}^{-1}$ and $\mathbf{Z}_{\mathrm{r,b}}^{-1}$ are found from (2.23), and $\boldsymbol{f}_{\mathrm{a}}^{\pm} = \boldsymbol{f}^{\pm}(z_1)$, $\boldsymbol{f}_{\mathrm{b}}^{\pm} = \boldsymbol{f}^{\pm}(z_N)$, as well as $\mathbf{P} = \mathbf{P}(z_N, z_1)$ have been introduced for brevity.

In analogy with the approach in [3] the modal split fields on either side of the structure are written in terms of the excitation fields $\boldsymbol{f}_{\mathrm{a}}^{+}$ and $\boldsymbol{f}_{\mathrm{b}}^{-}$ and the scattering matrix as

$$\begin{pmatrix} \boldsymbol{f}_{\mathrm{a}}^{+} \\ \boldsymbol{f}_{\mathrm{a}}^{-} \end{pmatrix} = \begin{pmatrix} \mathbf{I} & \mathbf{0} \\ \mathbf{S}_{11} & \mathbf{S}_{12} \end{pmatrix} \begin{pmatrix} \boldsymbol{f}_{\mathrm{a}}^{+} \\ \boldsymbol{f}_{\mathrm{b}}^{-} \end{pmatrix} = \left[\begin{pmatrix} \mathbf{I} & \mathbf{0} \\ \mathbf{0} & \mathbf{0} \end{pmatrix} + \begin{pmatrix} \mathbf{0} & \mathbf{0} \\ \mathbf{I} & \mathbf{0} \end{pmatrix} \begin{pmatrix} \mathbf{S}_{11} & \mathbf{S}_{12} \\ \mathbf{S}_{21} & \mathbf{S}_{22} \end{pmatrix} \right] \cdot \begin{pmatrix} \boldsymbol{f}_{\mathrm{a}}^{+} \\ \boldsymbol{f}_{\mathrm{b}}^{-} \end{pmatrix} \tag{2.34}$$

$$\begin{pmatrix} \boldsymbol{f}_{\mathrm{b}}^{+} \\ \boldsymbol{f}_{\mathrm{b}}^{-} \end{pmatrix} = \begin{pmatrix} \mathbf{S}_{21} & \mathbf{S}_{22} \\ \mathbf{0} & \mathbf{I} \end{pmatrix} \begin{pmatrix} \boldsymbol{f}_{\mathrm{a}}^{+} \\ \boldsymbol{f}_{\mathrm{b}}^{-} \end{pmatrix} = \left[\begin{pmatrix} \mathbf{0} & \mathbf{0} \\ \mathbf{0} & \mathbf{I} \end{pmatrix} + \begin{pmatrix} \mathbf{0} & \mathbf{I} \\ \mathbf{0} & \mathbf{0} \end{pmatrix} \cdot \begin{pmatrix} \mathbf{S}_{11} & \mathbf{S}_{12} \\ \mathbf{S}_{21} & \mathbf{S}_{22} \end{pmatrix} \right] \begin{pmatrix} \boldsymbol{f}_{\mathrm{a}}^{+} \\ \boldsymbol{f}_{\mathrm{b}}^{-} \end{pmatrix} \tag{2.35}$$

Insertion of these expressions in (2.33) yields a matrix equation

$$\left[\begin{pmatrix} \mathbf{0} & \mathbf{I} \\ \mathbf{0} & -\mathbf{Z}_{\mathrm{r,b}}^{-1} \end{pmatrix} - \mathbf{P} \begin{pmatrix} \mathbf{I} & \mathbf{0} \\ \mathbf{Z}_{\mathrm{r,a}}^{-1} & \mathbf{0} \end{pmatrix} \right] \begin{pmatrix} \mathbf{S}_{11} & \mathbf{S}_{12} \\ \mathbf{S}_{21} & \mathbf{S}_{22} \end{pmatrix} = \mathbf{P} \begin{pmatrix} \mathbf{I} & \mathbf{0} \\ -\mathbf{Z}_{\mathrm{r,a}}^{-1} & \mathbf{0} \end{pmatrix} - \begin{pmatrix} \mathbf{0} & \mathbf{I} \\ \mathbf{0} & \mathbf{Z}_{\mathrm{r,b}}^{-1} \end{pmatrix} \tag{2.36}$$

for arbitrary excitations $\boldsymbol{f}_{\mathrm{a}}^{+}$ and $\boldsymbol{f}_{\mathrm{b}}^{-}$. From this equation, one could solve directly for the scattering matrix $\mathbf{S}$, but this only leads to the instabilities as explored in detail

in [3]. Instead, we use the spectral decomposition (2.31) which enables separation of the exponentially growing and decaying terms in order to obtain a well-conditioned formulation *cf.*, (2.32). By following the technique in [3, pp. 33–34] the resulting generalized multimodal scattering matrix reads

$$\mathbf{S} = \begin{pmatrix} \mathbf{S}_{11} & \mathbf{S}_{12} \\ \mathbf{S}_{21} & \mathbf{S}_{22} \end{pmatrix} = \left[\mathbf{D}_- \mathbf{U}^\dagger \begin{pmatrix} \mathbf{0} & \mathbf{I} \\ \mathbf{0} & -\mathbf{Z}_{\mathrm{r,b}}^{-1} \end{pmatrix} - \mathbf{D}_+ \mathbf{U}^\dagger \begin{pmatrix} \mathbf{I} & \mathbf{0} \\ \mathbf{Z}_{\mathrm{r,a}}^{-1} & \mathbf{0} \end{pmatrix} \right]^{-1} \left[\mathbf{D}_+ \mathbf{U}^\dagger \begin{pmatrix} \mathbf{I} & \mathbf{0} \\ -\mathbf{Z}_{\mathrm{r,a}}^{-1} & \mathbf{0} \end{pmatrix} - \mathbf{D}_- \mathbf{U}^\dagger \begin{pmatrix} \mathbf{0} & \mathbf{I} \\ \mathbf{0} & \mathbf{Z}_{\mathrm{r,b}}^{-1} \end{pmatrix} \right] \tag{2.37}$$

where $\mathbf{D}_-$ and $\mathbf{D}_+$ are diagonal matrices found by identifying propagation factors that are both large and small which could correspond to any number of modes. For the sake of clarity we assume $|\mathrm{e}^{\mathrm{i}k_0 dn_m}| > 1$ for $m < k$, *i.e.*,

$$\mathbf{D}_- = \begin{pmatrix} \mathrm{e}^{-\mathrm{i}k_0 dn_1} & & & & & \\ & \ddots & & & & \\ & & \mathrm{e}^{-\mathrm{i}k_0 dn_{k-1}} & & & \\ & & & 1 & & \\ & & & & \ddots & \\ & & & & & 1 \end{pmatrix} \tag{2.38}$$

and

$$\mathbf{D}_+ = \begin{pmatrix} 1 & & & & & \\ & \ddots & & & & \\ & & 1 & & & \\ & & & \mathrm{e}^{\mathrm{i}k_0 dn_k} & & \\ & & & & \ddots & \\ & & & & & \mathrm{e}^{\mathrm{i}k_0 dn_n} \end{pmatrix} \tag{2.39}$$

Thus, by dividing by the potentially large exponential functions, all coefficients have finite amplitude leading to a well-conditioned scattering matrix form.

The technique in this section enables the computation of scattering matrices in a stable and numerically robust manner in all layers even where evanescent wave fields are present. Multilayer structures can be handled in a stable manner using the dissipative property of the Redheffer star product for cascading scattering matrices, see [3] for further details.

2.9 Reflection and transmission

The blocks of the scattering matrix, *e.g.*, (2.37) are by definition identified with the reflection and transmission matrices

$$\mathbf{S} = \begin{pmatrix} \mathbf{S}_{11} & \mathbf{S}_{12} \\ \mathbf{S}_{21} & \mathbf{S}_{22} \end{pmatrix} \tag{2.40}$$

By the scattering relation (2.28), we express the reflected and transmitted split fields in terms of (2.40). Thus, assuming incidence only from the left, *i.e.*, $\boldsymbol{f}^{-}(z_N) = \mathbf{0}$, we get

$$\begin{cases} \boldsymbol{f}^{-}(z_0) = \mathbf{S}_{11}\boldsymbol{f}^{+}(z_0) \\ \boldsymbol{f}^{+}(z_N) = \mathbf{S}_{21}\boldsymbol{f}^{+}(z_0) \end{cases} \tag{2.41}$$

The split fields $\boldsymbol{f}^{\pm}$ can in fact be identified with the electric harmonics $\boldsymbol{s}_{\mathrm{t}}$ as seen by combination of (2.22) with (2.20). The result is

$$\boldsymbol{f}^{\pm} = \frac{1}{2}(\boldsymbol{s}_{\mathrm{t}} \mp \mathbf{Z}_{\mathrm{r}}\boldsymbol{u}_{\mathrm{t}}) = \frac{1}{2}(\boldsymbol{s}_{\mathrm{t}} + \boldsymbol{s}_{\mathrm{t}}) = \boldsymbol{s}_{\mathrm{t}} \tag{2.42}$$

Thus, (2.41) can be rewritten in terms of the electric harmonics according to

$$\begin{cases} \boldsymbol{s}_{\mathrm{t}}^{\mathrm{ref}}(z_0) = \mathbf{S}_{11}\boldsymbol{s}_{\mathrm{t}}^{\mathrm{inc}}(z_0) \\ \boldsymbol{s}_{\mathrm{t}}^{\mathrm{trn}}(z_N) = \mathbf{S}_{21}\boldsymbol{s}_{\mathrm{t}}^{\mathrm{inc}}(z_0) \end{cases} \tag{2.43}$$

where $\boldsymbol{s}_{\mathrm{t}}^{\mathrm{inc}}$ denotes the spatial harmonic of the incident electric source field.

Assume that the sources located at the left side of the structure depicted in Figure 1, generates a source field in terms of a single monochromatic plane wave propagating in the direction $\hat{\boldsymbol{k}} = \boldsymbol{k}(0,0)/|\boldsymbol{k}(0,0)|$ ($|\theta| < 90^{\circ}$), with unit amplitude polarization $\boldsymbol{E}_0$ at the plane $z = z_0$, thus

$$\boldsymbol{s}_{\mathrm{t}}^{\mathrm{inc}} = \begin{pmatrix} E_{0,\mathrm{x}}\boldsymbol{\delta}_{00,pq} \\ E_{0,\mathrm{y}}\boldsymbol{\delta}_{00,pq} \end{pmatrix} \quad \text{and} \quad \boldsymbol{\delta}_{00,pq} = \begin{pmatrix} 0 \\ \vdots \\ 0 \\ \delta_{00,pq} \\ 0 \\ \vdots \\ 0 \end{pmatrix} \tag{2.44}$$

where the column vector $\boldsymbol{\delta}_{00,pq}$ is of length $(2P+1)(2Q+1)$, and $\delta_{00,pq}$, denote the Kronecker delta. The polarization vector can be written in terms of a polarization angle χ ($\chi = 0$ TE and $\chi = \pi/2$ TM) according to

$$\boldsymbol{E}_0(z_0) = E_0(z_0)(\hat{\boldsymbol{e}}_{\perp}\cos\chi + \hat{\boldsymbol{e}}_{\parallel}\sin\chi) \tag{2.45}$$

where $|\boldsymbol{E}_0(z_0)| = 1$, $\hat{\boldsymbol{e}}_{\perp} = \hat{\boldsymbol{z}} \times \hat{\boldsymbol{k}}(0,0)$, and $\hat{\boldsymbol{e}}_{\parallel} = \hat{\boldsymbol{k}}(0,0) \times \hat{\boldsymbol{e}}_{\perp}$, whereas $\hat{\boldsymbol{k}}(0,0) = \boldsymbol{k}(0,0)/|\boldsymbol{k}(0,0)|$ with $\boldsymbol{k}$ found from (2.6). In the case of normal incidence $\hat{\boldsymbol{z}}$ and $\hat{\boldsymbol{k}}(0,0)$ are parallel and then $\hat{\boldsymbol{e}}_{\perp}$ is arbitrarily set to $\hat{\boldsymbol{y}}$. It should be noticed that extensions of the classical RCWA formulation have been made for the handling of more general source fields in a way that it can propagate multiple input modes in a single calculation see, [7]. For arbitrary linear homogeneous isotropic media a on the left and b on the right, *cf.*, Figure 1, we express the incident, reflected and

transmitted time averaged power flow according to

$$\begin{cases} \mathcal{P}_{\mathrm{z}}^{\mathrm{inc}} = \dfrac{1}{2\eta_0}\,\mathrm{Re}\,\{\dfrac{k_{\mathrm{z,a}}^{\mathrm{inc}}}{\mu_{\mathrm{a}}k_0}\}|\boldsymbol{s}^{\mathrm{inc}}(0,0,z_0)|^2 \\ \mathcal{P}_{\mathrm{z}}^{\mathrm{ref}} = -\dfrac{1}{2\eta_0}\displaystyle\sum_{p,q}\mathrm{Re}\,\{\dfrac{k_{\mathrm{z,a}}(p,q)}{\mu_{\mathrm{a}}k_0}\}|\boldsymbol{s}^{\mathrm{ref}}(p,q,z_0)|^2 \\ \mathcal{P}_{\mathrm{z}}^{\mathrm{trn}} = \dfrac{1}{2\eta_0}\displaystyle\sum_{p,q}\mathrm{Re}\,\{\dfrac{k_{\mathrm{z,b}}(p,q)}{\mu_{\mathrm{b}}k_0}\}|\boldsymbol{s}^{\mathrm{trn}}(p,q,z_N)|^2 \end{cases} \tag{2.46}$$

where

$$\boldsymbol{s}^{\mathrm{inc}} = \begin{pmatrix} \boldsymbol{s}_{\mathrm{x}}^{\mathrm{inc}} \\ \boldsymbol{s}_{\mathrm{y}}^{\mathrm{inc}} \\ \boldsymbol{s}_{\mathrm{z}}^{\mathrm{inc}} \end{pmatrix}, \quad \boldsymbol{s}^{\mathrm{ref}} = \begin{pmatrix} \boldsymbol{s}_{\mathrm{x}}^{\mathrm{ref}} \\ \boldsymbol{s}_{\mathrm{y}}^{\mathrm{ref}} \\ \boldsymbol{s}_{\mathrm{z}}^{\mathrm{ref}} \end{pmatrix} \quad \text{and} \quad \boldsymbol{s}^{\mathrm{trn}} = \begin{pmatrix} \boldsymbol{s}_{\mathrm{x}}^{\mathrm{trn}} \\ \boldsymbol{s}_{\mathrm{y}}^{\mathrm{trn}} \\ \boldsymbol{s}_{\mathrm{z}}^{\mathrm{trn}} \end{pmatrix} \tag{2.47}$$

with the longitudinal amplitude vector components computed according to

$$\begin{cases} \boldsymbol{s}_{\mathrm{z}}^{\mathrm{inc}} = -\mathbf{K}_{\mathrm{z,a}}^{-1}\big(\mathbf{K}_{\mathrm{x}}\boldsymbol{s}_{\mathrm{x}}^{\mathrm{inc}} + \mathbf{K}_{\mathrm{y}}\boldsymbol{s}_{\mathrm{y}}^{\mathrm{inc}}\big) \\ \boldsymbol{s}_{\mathrm{z}}^{\mathrm{ref}} = \mathbf{K}_{\mathrm{z,a}}^{-1}\big(\mathbf{K}_{\mathrm{x}}\boldsymbol{s}_{\mathrm{x}}^{\mathrm{ref}} + \mathbf{K}_{\mathrm{y}}\boldsymbol{s}_{\mathrm{y}}^{\mathrm{ref}}\big) \\ \boldsymbol{s}_{\mathrm{z}}^{\mathrm{trn}} = -\mathbf{K}_{\mathrm{z,b}}^{-1}\big(\mathbf{K}_{\mathrm{x}}\boldsymbol{s}_{\mathrm{x}}^{\mathrm{trn}} + \mathbf{K}_{\mathrm{y}}\boldsymbol{s}_{\mathrm{y}}^{\mathrm{trn}}\big) \end{cases} \tag{2.48}$$

where

$$\mathbf{K}_{\mathrm{z,r}} = (\mu_{\mathrm{r}}\epsilon_{\mathrm{r}}\mathbf{I} - \mathbf{K}_{\mathrm{x}}^2 - \mathbf{K}_{\mathrm{y}}^2)^{1/2}, \quad r = a, b \tag{2.49}$$

By assuming incidence from the left, *cf.*, Figure 1, the overall reflectance and transmissivity are ($|\boldsymbol{s}^{\mathrm{inc}}|^2 = 1$)

$$\begin{cases} R = \displaystyle\sum_{p,q}\mathrm{Re}\,\{\dfrac{k_{\mathrm{z,a}}(p,q)}{k_{\mathrm{z,a}}^{\mathrm{inc}}}\}|\boldsymbol{s}^{\mathrm{ref}}(p,q,z_0)|^2 \\ T = \displaystyle\sum_{p,q}\mathrm{Re}\,\{\dfrac{\mu_{\mathrm{a}}}{\mu_{\mathrm{b}}}\dfrac{k_{\mathrm{z,b}}(p,q)}{k_{\mathrm{z,a}}^{\mathrm{inc}}}\}|\boldsymbol{s}^{\mathrm{trn}}(p,q,z_N)|^2 \end{cases} \tag{2.50}$$

where

$$\begin{cases} |\boldsymbol{s}^{\mathrm{ref}}|^2 = |\boldsymbol{s}_{\mathrm{x}}^{\mathrm{ref}}|^2 + |\boldsymbol{s}_{\mathrm{y}}^{\mathrm{ref}}|^2 + |\boldsymbol{s}_{\mathrm{z}}^{\mathrm{ref}}|^2 \\ |\boldsymbol{s}^{\mathrm{trn}}|^2 = |\boldsymbol{s}_{\mathrm{x}}^{\mathrm{trn}}|^2 + |\boldsymbol{s}_{\mathrm{y}}^{\mathrm{trn}}|^2 + |\boldsymbol{s}_{\mathrm{z}}^{\mathrm{trn}}|^2 \end{cases} \tag{2.51}$$

for each p, q. The sum of R and T must be unity for lossless gratings *i.e.*, energy conservation shall be maintained. This condition is necessary for lossless structures but not sufficient to ensure the accuracy of the diffraction efficiency, [36, pp. 1074–1076].

Thus, the total reflectance and transmissivity, *i.e.*, the diffraction efficiency is defined by (2.50) where the sums are over all diffraction orders. Corresponding specular reflectance and transmissivity, respectively are found by just taking the zero order terms ($p = q = 0$) in (2.50). In general, the reflected and transmitted diffraction efficiencies of order (p, q) are given by

$$\begin{aligned} \mathrm{DE}_{\mathrm{R}}(p,q) &= \mathrm{Re}\,\{\frac{k_{\mathrm{z,a}}(p,q)}{k_{\mathrm{z,a}}^{\mathrm{inc}}}\}|\boldsymbol{s}^{\mathrm{ref}}(p,q,z_0)|^2 \\ \mathrm{DE}_{\mathrm{T}}(p,q) &= \mathrm{Re}\,\{\frac{\mu_{\mathrm{a}}}{\mu_{\mathrm{b}}}\frac{k_{\mathrm{z,b}}(p,q)}{k_{\mathrm{z,a}}^{\mathrm{inc}}}\}|\boldsymbol{s}^{\mathrm{trn}}(p,q,z_N)|^2 \end{aligned} \tag{2.52}$$

for fixed p and q.

3 Potential extensions

FMM is in general a versatile and robust class of methods well adapted for grating diffraction problems. Unfortunately, it requires the solution of an eigenproblem which becomes particularly costly in the case of two-dimensional crossed gratings, where the number of retained orders are squared relative to the one-dimensional (1D) grating. As mentioned in the Introduction several improvements have been introduced for FMM in the past decades with focus on convergence and accuracy improvements [30].

Besides stability issues [27, 37] crucial steps towards accurate and fast converging schemes, *e.g.*, the application of the correct factorization rules and fast Fourier factorization introduced in [33, 39], further developed for two-dimensional crossed gratings [26] as well as gratings with anisotropic materials [28, 32, 41]. Improved convergence rates have also been obtained through reformulation of FMM with adaptive spatial resolution (ASR) techniques as was done in [17] for one-dimensional gratings and later generalized for multilevel profiles [51] as well as two-dimensional crossed gratings [19]. A method that automatically generates adaptive coordinates (AC) for arbitrarily shaped index profiles has been proposed in [14]. The AC and ASR techniques support more accurate resolutions regarding small geometric features and/or large refractive index contrasts within the reference cell. The factorization rules have in addition been combined with the normal vector method in order to handle more general geometries of the refractive index contrast [9, 15, 47]. Recently, [52] and [11] provided a local normal vector field approach that makes use of the gradient of the real permittivity in the reference cell in order to generate local normal vectors.

Methods based on polynomials and non-periodic basis function expansions have furthermore been considered as alternative techniques for stability and convergence rate improvement, [12, 13, 24, 59]. An alternative approach to suppress the Gibbs phenomenon is to treat continuous field components in the Fourier space analogously to the conventional algorithm, whereas the discontinuous components are calculated in real space as suggested by [5]. In addition [49] recently proposed an alternative treatment of interface conditions to overcome the effect of the Gibbs phenomenon that is crucial, *e.g.*, for accurate near field computations.

Thus, these techniques are potential extensions for methods based on FMM that have been proven useful, *e.g.*, in order to handle gratings with ultrahigh-contrast permittivity profile within the optical regime [17, 18, 51, 57] or metallic lamellar gratings at microwave frequencies [22, 23] as well as plasmonic resonances [56]. However, this paper is limited to consider an alternative FMM formulation that classically make use of Fourier expansions of the electromagnetic fields and on grating parameters while being based on scattering matrices that rely on stabilized wave propagation operators [3]. The new scheme is adapted for layered and periodic dielectric devices with moderate to low index contrast.

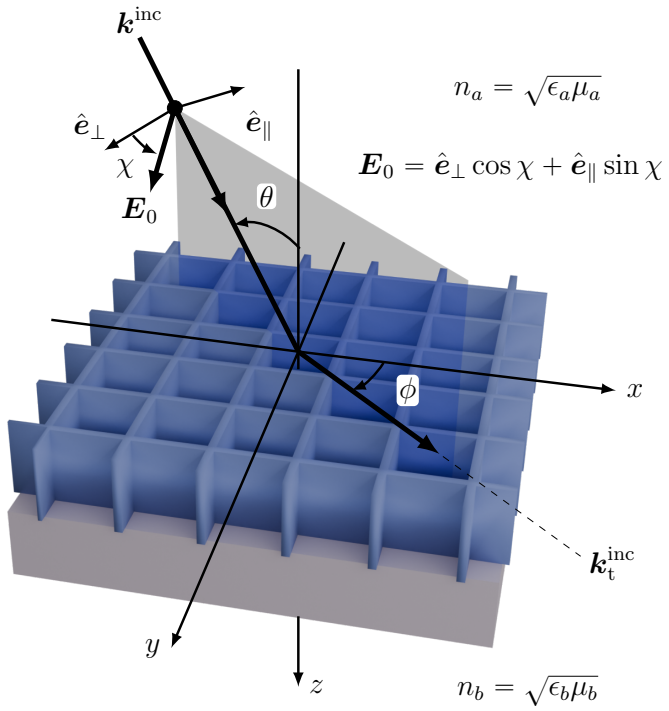

Figure 2: Scattering configuration. The plane of incidence is illustrated by a grey shaded rectangle. The normal of the plane of incidence is parallel with $\hat{\boldsymbol{e}}_\perp$ and the field polarization angle is χ. For $\chi = 0$ (TE) and $\chi = \pi/2$ (TM) the electric and the magnetic fields, respectively, are perpendicular to the plane of incidence.

4 Numerical examples

This section provides three examples for verification and demonstration purpose regarding the efficiency and accuracy of the proposed method. As stated in the Introduction the main focus in this paper is on periodic structures made of dielectrics with moderate to low index contrast having interest, *e.g.*, in the microwave regime for the electrical design of broad band gradient radomes [42]. To this end examples of practical interest have been chosen with moderate as well as low index profiles. The last example considers benchmarking of the proposed method for analysis of an anisotropic grating earlier presented in [16, 21, 28]. This last example is of importance for the preparation of future development and generalizations *e.g.*, in order to adapt the method to more complex configurations.

In the numerical examples, a linearly polarized time-harmonic electromagnetic plane wave is incident upon a binary dielectric grating structure, as depicted in Figure 2. The wave propagates in the direction of the incident wave vector $\boldsymbol{k}^{\mathrm{inc}} = \boldsymbol{k}(0,0)$, see (2.6), at angle of incidence $\theta \in [0^\circ, 90^\circ)$, and azimuth angle $\phi \in [0^\circ, 360^\circ)$, defined by the angle between the x-axis and the projection of the incident wave vector $\boldsymbol{k}^{\mathrm{inc}}$ on the xy-plane. The polarization angle between the electric-field vector $\boldsymbol{E}_0$ and the normal $\hat{\boldsymbol{e}}_\perp$ to the plane of incidence is denoted by χ, see (2.45) and Figure 2.

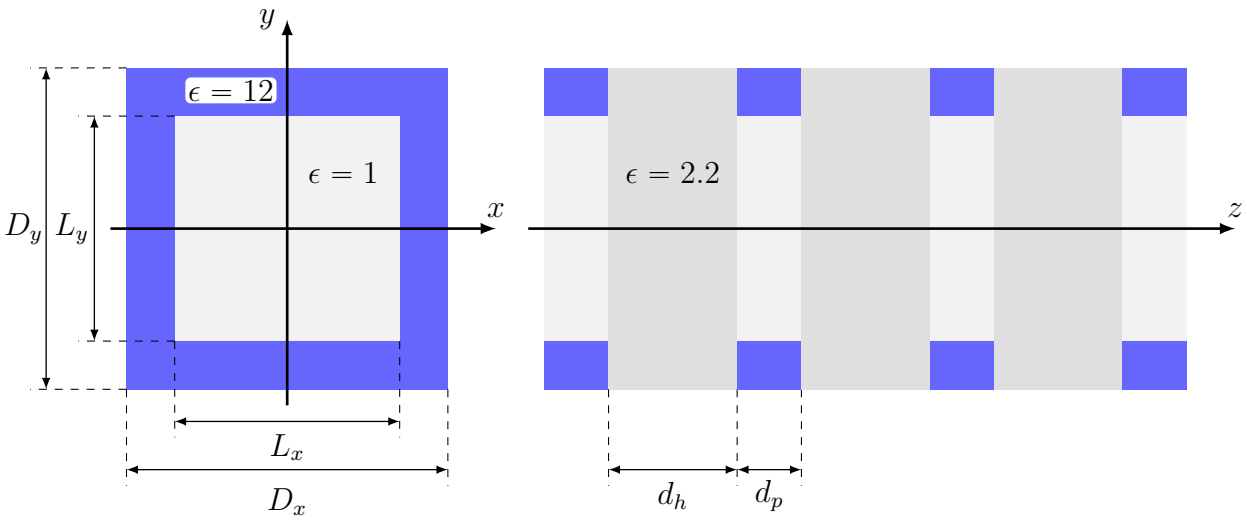

Figure 3: The geometry of the 7-layer binary grating [6, 54, 55]. The three gray shaded slabs represent the homogeneous layers with thickness $d_h = 4$ mm and relative permittivity $\epsilon = 2.2$, whilst the other slabs represent the 2D periodic layers with thickness $d_p = 2$ mm made of a material with relative permittivity $\epsilon = 12$ indicated by blue shaded regions. The reference cells are rectangular having periods $D_x = D_y = 10$ mm and centered quadratic air filled holes of side lengths $L_x = L_y = 7$ mm.

4.1 Multilayer binary crossed grating

The device considered is a 7-layer lossless dielectric binary crossed grating earlier presented in [6, 54, 55]. More specifically, the structure as depicted in Figure 3, is made up by three identical homogeneous layers and four identical 2D-periodic grating layers. Computed diffraction efficiency using the proposed FMM formulation is presented in Figure 4. The result agrees well with corresponding HFSS reference solution produced by using a frequency domain finite element method (FEM). However, a slight shift of the frequency response is observed in Figure 4 indicating that the solution has not fully been converged for $P = Q = 9$. The slight deviation can also be seen in Figure 5 presenting the convergence rate and relative error at the fixed frequency 9.0 GHz. The calculation time for the FMM formulation using truncation order $P = Q = 9$ and implemented in MATLAB was approximately 10 times faster than corresponding HFSS FEM solution. The calculation time as a function of truncation order agrees well with corresponding results reported in [55, Fig. 3. (d)]. The convergence rate in Figure 5 corresponds well with data computed by use of the enhanced transfer matrix method (ETM) reported in [54, Figure 5 (a)]. However, corresponding convergence results by use of adaptive spatial resolution (ASR) given in [54, Figure 5 (a)] showed limited computational precision for truncation orders above 22 which is not the case by use of the method of this paper, see Figure 5. Thus, this result indicates that the proposed formulation handles higher order modes in a robust and stable manner.

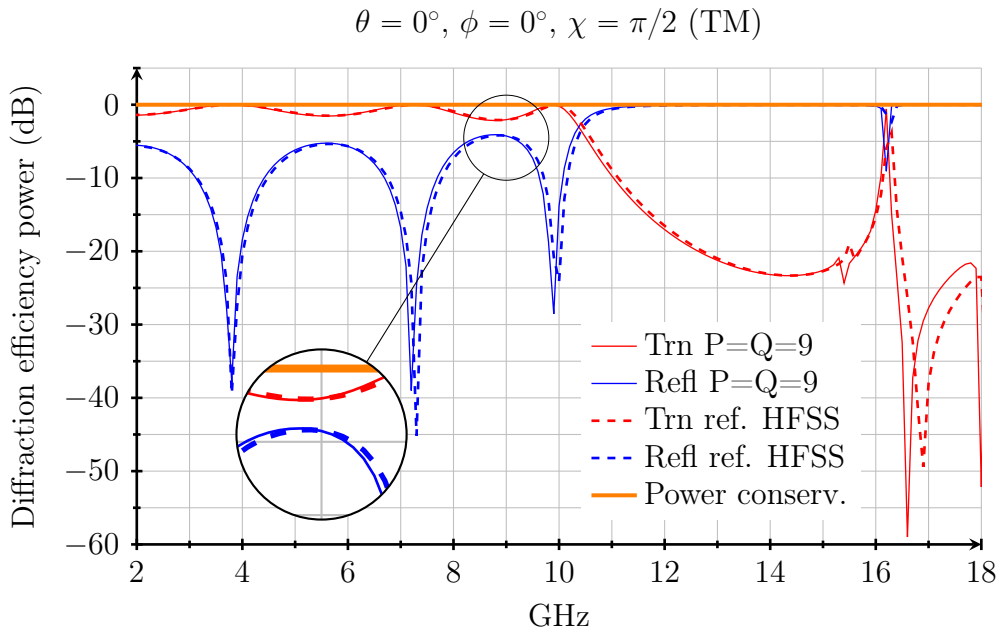

Figure 4: Diffraction efficiency (2.50) of the 7-layer binary grating [54]. Incidence TM polarization ($\chi = \pi/2$) at normal angles of incidence, *i.e.*, $\theta = 0°$ and $\phi = 0°$.

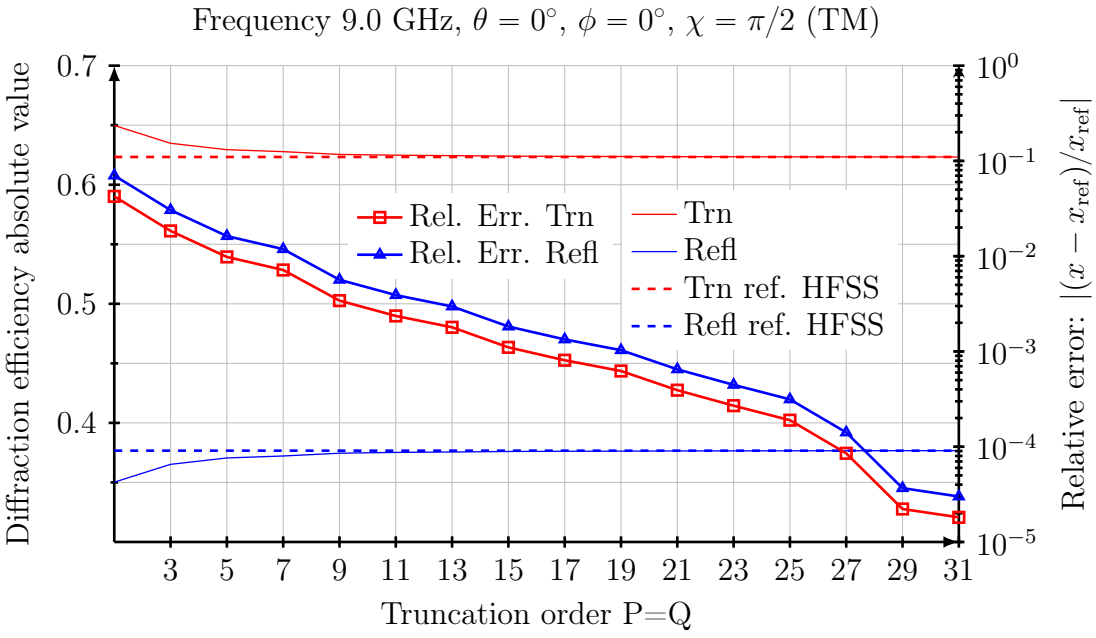

Figure 5: The convergence rate and relative error of the diffraction efficiency (2.50) at 9 GHz for the 7-layer binary grating. The reference has been computed by Ansys HFSS.

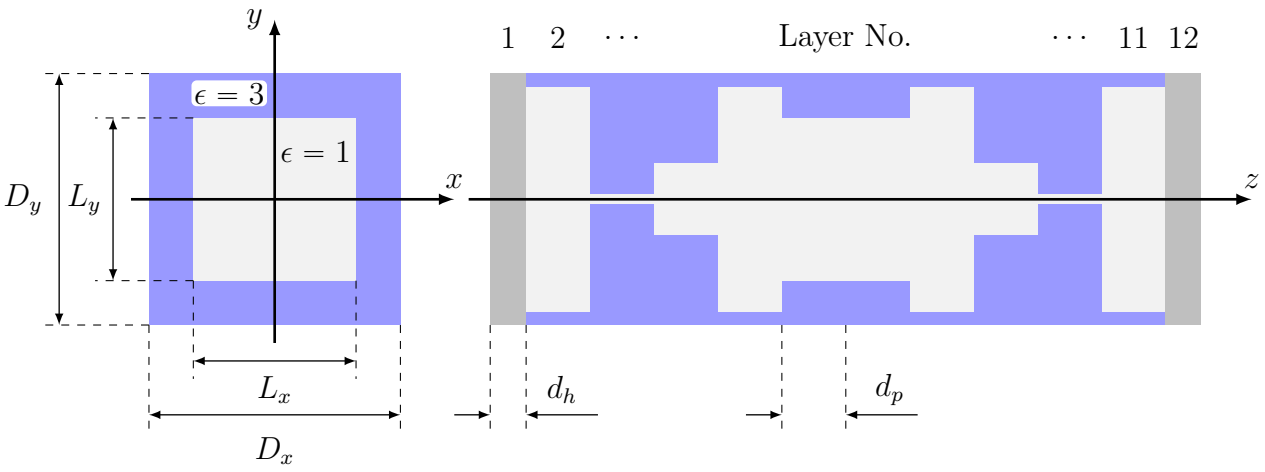

Figure 6: The geometry of the gradient radome. The gray shaded layers (layer number 1 and 12) represent the homogeneous layers with permittivity $\epsilon = 3.50$ and thickness $d_h = 1$ mm enclosing the interior stack of 2D periodic layers (layer number 2−11). The reference cell is made of a material with permittivity $\epsilon = 3$ with period $D_x = D_y = 7.00$ mm. The cells having air filled square holes of side lengths $L_x = L_y$ in accordance with values given in Table 1. The thickness of the 2D-periodic layers are all identical and equal $d_p = 1.78$ mm.

4.2 Broadband gradient radome

This example considers a gradient radome based on a dielectric 2D periodic gradient structure with broadband characteristics [43]. The considered radome design constitutes of two homogeneous layers enclosing an interior stack of 2D periodic dielectric binary crossed grating layers. All materials are assumed being lossless in this example. The structure and design parameters of the radome are defined in Figure 6 and Table 1. Notice that this is a relevant numerical example, however any discussion on the optimization technique as well as realization aspects *e.g.*, by use of 3D printing technology is out of the scope of this paper. Figure 7 shows the diffraction efficiency of the gradient radome.

As seen in Figure 7, computed results by use of the proposed method agree very well with the reference solution, even with a relatively low order truncation ($P = Q = 5$). Corresponding convergence performance is presented in Figure 8.

From Figure 8 it is seen that the relative error for transmission and reflection are identical for TE polarization which is due to the fact that both the reflection and transmission level coincides (all materials assumed lossless) around −5 dB at 8.5 GHz according to Figure 7. However, this is not the case for TM polarization where the reflection level is approximately −10 dB lower relative corresponding transmission data *cf.*, Figure 7, which implies larger relative error of the reflection data relative corresponding transmission data as clearly is shown in Figure 8.

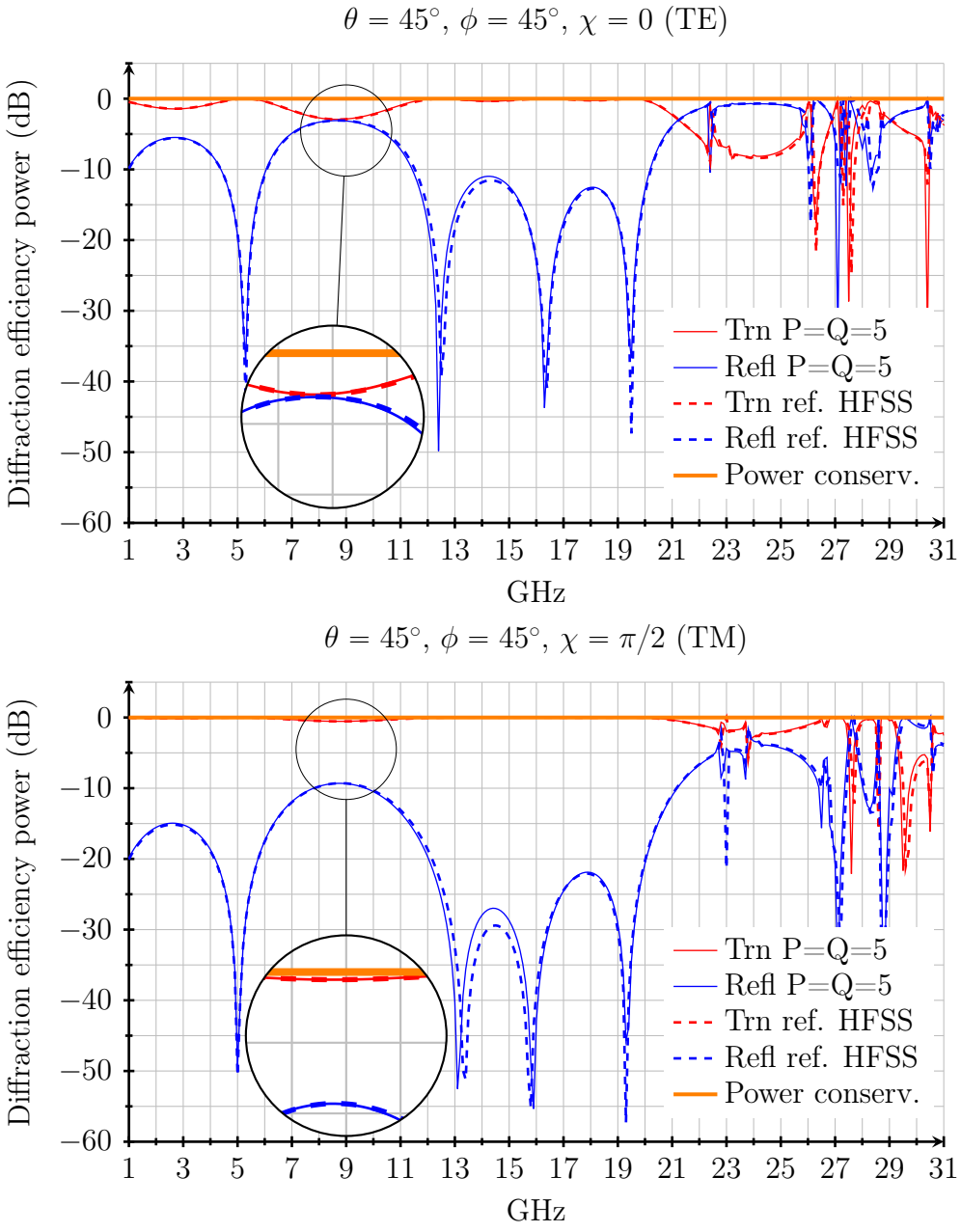

Figure 7: Diffraction efficiency (2.50) of the broad band gradient radome defined in Figure 6 and Table 1. Incidence TE ($\chi = 0$) and TM polarization ($\chi = \pi/2$), respectively, at oblique angles of incidence $\theta = 45^\circ$ and $\phi = 45^\circ$.

Layer No.	$L_x = L_y$ [mm]	Remark	Layer No.	$L_x = L_y$ [mm]	Remark
1	-	Hom.	7	4.53	2D-per.
2	6.25	2D-per.	8	6.25	2D-per.
3	0.25	2D-per.	9	2.00	2D-per.
4	2.00	2D-per.	10	0.25	2D-per.
5	6.25	2D-per.	11	6.25	2D-per.
6	4.53	2D-per.	12	–	Hom.

Table 1: The side lengths $L_x = L_y$ of the dielectric square binary crossed grating layers *i.e.*, layer number 2−11. Layer number 1 and 12 are the enclosing homogeneous layers of the gradient radome *cf.*, Figure 6.

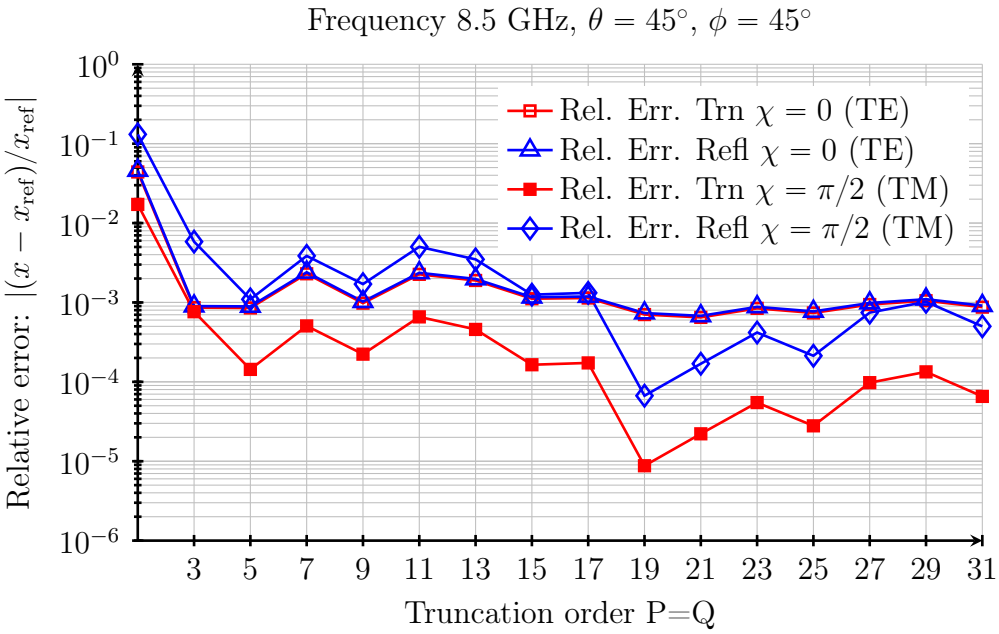

Figure 8: The relative error of the diffraction efficiency (2.50) at 8.5 GHz for the gradient radome. The reference has been computed by Ansys HFSS.

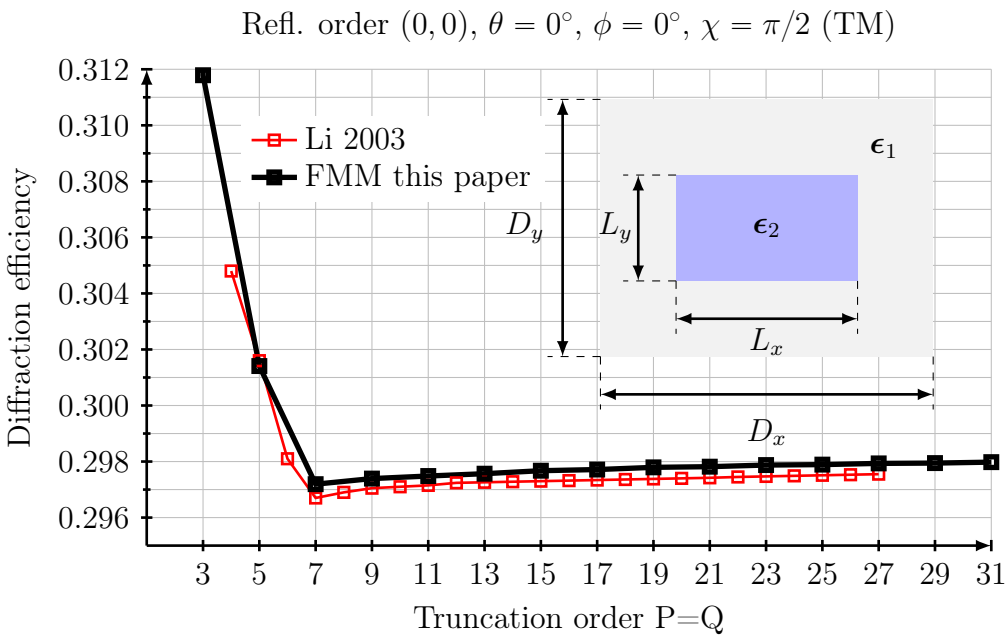

Figure 9: Convergence rate of the zero order diffraction efficiency $\mathrm{DE}_{\mathrm{R}}(0,0)$ in (2.52) of the anisotropic crossed grating with grating parameters, $D_x = 2.4\lambda_0$, $D_y = 1.4\lambda_0$, $L_x/D_x = L_y/D_y = 0.5$, and thickness λ_0 (an arbitrary free space wavelength), see [28, p.352] for details. The polarization is TM ($\chi = \pi/2$), at normal angle of incidence $\theta = 0^\circ$ and $\phi = 0^\circ$, *i.e.*, the incident electric field vector is aligned along the x axis *cf.*, Figure 2.

4.3 Anisotropic binary crossed grating

This last example considers a binary crossed anisotropic grating earlier reported in [28]. The grating is nonmagnetic *i.e.*, $\boldsymbol{\mu} = \mathbf{I}$ and is described by two gyrotropic anisotropic permittivity tensors given by

$$\boldsymbol{\epsilon}_1 = \begin{pmatrix} 2.25 & \mathrm{i}0.5 & 0 \\ -\mathrm{i}0.5 & 2.25 & 0 \\ 0 & 0 & 2 \end{pmatrix} \quad \text{and} \quad \boldsymbol{\epsilon}_2 = \begin{pmatrix} 2.25 & -\mathrm{i}0.5 & 0 \\ \mathrm{i}0.5 & 2.25 & 0 \\ 0 & 0 & 2 \end{pmatrix} \tag{4.1}$$

The semi-infinite media to the left and right enclosing the grating are described by refractive index $n_a = 1$ and $n_b = 1 + \mathrm{i}5$, respectively, *cf.*, Figure 1 or 2.

The convergence rate result for the grating using the formulation proposed in this paper is shown in Figure 9. The numerical result in Figure 9 agrees well with the corresponding case computed without use of the factorization procedure as reported in [28, p.352] and reproduced in Figure 9 for convenience. In addition, see also corresponding results reported in [21, p. 1705] that used a *projection operator* method which is a variation of the normal-vector method as well as [16, p.656–657] that used a modal *spectral element method* (SEM) with modified Legendre polynomials to analyze binary crossed gratings.

5 Conclusions

The proposed multimodal formulation is a semi-analytical FMM method that classically relies on plane-wave expansions of the electromagnetic fields and on grating parameters such as the permittivity and the permeability. The new method is closely related to classical RCWA built on scattering matrices [46], however a key difference is that the proposed scheme relies on the recently reported concept of stabilized wave propagation operators that enhance numerical stability.

The new formulation can handle anisotropic gratings and functional devices made of periodic multilayer dielectrics having moderate to low index contrast corresponding to materials ranging from conventional dielectric 3D printing materials to ceramic materials. Through numerical examples it has been demonstrated that even with a relatively low order truncation, computed results with the proposed method showed excellent agreement with corresponding reference solutions computed by FEM, with maximum relative error sufficiently low for usage in the design process of a broad range of practical applications. While FEM is a versatile method, the proposed semi-analytical approach offers significant advantage in terms of computational efficiency. The numerical efficiency and accuracy showed in fact similar performance in comparison with related schemes recently reported in the literature. The dissipation property of the Redheffer star product, furthermore implies that multilayer devices can be handled in a numerically stable manner which makes the method useful for a broad class of problems where evanescent fields are present. It was demonstrated that the proposed method did not suffer from numerical instabilities for large truncation orders which is an advantage compared with the corresponding results published in [54].

The proposed formulation is well suited as a design tool in combination with any optimization toolbox supported by, *e.g.*, MATLAB or similar. Another application could be a tool for creating reflection and transmission data characterizing any 2D periodic dielectric device as input to solvers based on high frequency approximations adapted for the analysis of scattering properties of electrically large structures that is common in, *e.g.*, the microwave regime for electrical design and optimization of radomes [1, 2].

In addition there is potential for improving convergence rate and accuracy further by incorporating techniques such as correct factorization rules, adaptive spatial resolution or the use of polynomials and non-periodic basis function expansions. These extensions are crucial in order to handle gratings with, *e.g.*, ultrahigh-contrast permittivity profile such as metallic lamellar gratings at microwave frequencies. However, these techniques have not been introduced within the scope of this paper.

Finally, the proposed approach is well prepared for further development by the fact that it is formulated for general dielectric anisotropic 2D gratings and based on the general framework of scattering matrices that supports the incorporation of other methods and techniques as pointed out in [46].

Acknowledgments

The work reported in this paper was supported by grants from Saab Dynamics AB, Linköping, Sweden, which is gratefully acknowledged. The authors also would like to thank Dr. Christer Larsson from Saab Dynamics AB, for the support and helpful discussions about the content of this paper.

References

[1] M. Andersson. "Higher order scattering contributions with surface integral representations for radome analysis". In: *URSI GASS 2021, Rome, Italy, 28 August - 4 September 2021*. URSI. 2021.

[2] M. Andersson. "Plane wave spectrum in radome applications". In: *2019 International Conference on Electromagnetics in Advanced Applications (ICEAA)*. IEEE. 2019, pp. 0453–0458.

[3] M. Andersson, D. Sjöberg, and G. Kristensson. "Stabilization of evanescent wave propagation operators". *Progress In Electromagnetics Research B* 101 (2023): pp. 17–44.

[4] B. Anić. "The Fourier-Galerkin Method for Band Structure Computations of 2D and 3D Photonic Crystals". PhD thesis. Karlsruher Institut für Technologie (KIT), 2013.

[5] R. Antos and M. Veis. "Coupled wave method with modified boundary conditions for diffraction grating calculations". *Japanese Journal of Applied Physics* 59 (SE) (2020): SEEB02.

[6] A. Attiya and A. Kishk. "Modal analysis of a two-dimensional dielectric grating slab excited by an obliquely incident plane wave". *Progress In Electromagnetics Research* 60 (2006): pp. 221–243.

[7] M. Auer and K.-H. Brenner. "Localized input fields in rigorous coupled-wave analysis". *JOSA A* 31 (11) (2014): pp. 2385–2393.

[8] M. Auslender and S. Hava. "Scattering-matrix propagation algorithm in full-vectorial optics of multilayer grating structures". *Optics letters* 21 (21) (1996): pp. 1765–1767.

[9] J. Bischoff. "Formulation of the normal vector RCWA for symmetric crossed gratings in symmetric mountings". *JOSA A* 27 (5) (2010): pp. 1024–1031.

[10] N. Cotter, T. Preist, and J. Sambles. "Scattering-matrix approach to multilayer diffraction". *JOSA A* 12 (5) (1995): pp. 1097–1103.

[11] P. S. Davids. "Normal vector approach to Fourier modal scattering from planar periodic photonic structures". *Photonics and Nanostructures-Fundamentals and Applications* 43 (2021): p. 100864.

[12] K. Edee. "Modal method based on subsectional Gegenbauer polynomial expansion for lamellar gratings". *JOSA A* 28 (10) (2011): pp. 2006–2013.

[13] K. Edee and J. Plumey. "Numerical scheme for the modal method based on subsectional Gegenbauer polynomial expansion: application to biperiodic binary grating". *JOSA A* 32 (3) (2015): pp. 402–410.

[14] S. Essig and K. Busch. "Generation of adaptive coordinates and their use in the Fourier modal method". *Optics Express* 18 (22) (2010): pp. 23258–23274.

[15] P. Götz, T. Schuster, K. Frenner, S. Rafler, and W. Osten. "Normal vector method for the RCWA with automated vector field generation". *Optics express* 16 (22) (2008): pp. 17295–17301.

[16] G. Granet. "Modal spectral element method with modified Legendre polynomials to analyze binary crossed gratings". *JOSA A* 40 (4) (2023): pp. 652–660.

[17] G. Granet. "Reformulation of the lamellar grating problem through the concept of adaptive spatial resolution". *JOSA A* 16 (10) (1999): pp. 2510–2516.

[18] G. Granet, J. Chandezon, J.-P. Plumey, and K. Raniriharinosy. "Reformulation of the coordinate transformation method through the concept of adaptive spatial resolution. application to trapezoidal gratings". *JOSA A* 18 (9) (2001): pp. 2102–2108.

[19] G. Granet and J.-P. Plumey. "Parametric formulation of the Fourier modal method for crossed surface-relief gratings". *Journal of Optics A: Pure and Applied Optics* 4 (5) (2002): S145.

[20] J. J. Hench and Z. Strakoš. "The RCWA method-a case study with open questions and perspectives of algebraic computations". *Electronic Transactions on Numerical Analysis* 31 (2008): pp. 331–357.

[21] K. C. Johnson. "Projection operator method for biperiodic diffraction gratings with anisotropic/bianisotropic generalizations". *JOSA A* 31 (8) (2014): pp. 1698–1709.

[22] A. Khavasi and K. Mehrany. "Adaptive spatial resolution in fast, efficient, and stable analysis of metallic lamellar gratings at microwave frequencies". *IEEE Transactions on Antennas and Propagation* 57 (4) (2009): pp. 1115–1121.

[23] A. Khavasi and K. Mehrany. "Regularization of jump points in applying the adaptive spatial resolution technique". *Optics Communications* 284 (13) (2011): pp. 3211–3215.

[24] A. Khavasi, K. Mehrany, and B. Rashidian. "Three-dimensional diffraction analysis of gratings based on Legendre expansion of electromagnetic fields". *JOSA B* 24 (10) (2007): pp. 2676–2685.

[25] G. Kristensson. "Scattering of Electromagnetic Waves by Obstacles". Mario Boella Series on Electromagnetism in Information and Communication. SciTech Publishing, 2016.

[26] P. Lalanne. "Improved formulation of the coupled-wave method for two-dimensional gratings". *JOSA A* 14 (7) (1997): pp. 1592–1598.

[27] L. Li. "Formulation and comparison of two recursive matrix algorithms for modeling layered diffraction gratings". *JOSA A* 13 (5) (1996): pp. 1024–1035.

[28] L. Li. "Fourier modal method for crossed anisotropic gratings with arbitrary permittivity and permeability tensors". *Journal of Optics A: Pure and Applied Optics* 5 (4) (2003): p. 345.

[29] L. Li. "Justification of matrix truncation in the modal methods of diffraction gratings". *Journal of Optics A: Pure and Applied Optics* 1 (4) (1999): p. 531.

[30] L. Li. "Mathematical reflections on the Fourier modal method in grating theory". In: *Mathematical modeling in optical science*. SIAM, 2001, pp. 111–139.

[31] L. Li. "New formulation of the Fourier modal method for crossed surface-relief gratings". *JOSA A* 14 (10) (1997): pp. 2758–2767.

[32] L. Li. "Reformulation of the Fourier modal method for surface-relief gratings made with anisotropic materials". *Journal of Modern Optics* 45 (7) (1998): pp. 1313–1334.

[33] L. Li. "Use of Fourier series in the analysis of discontinuous periodic structures". *JOSA A* 13 (9) (1996): pp. 1870–1876.

[34] V. Liu and S. Fan. "S4: a free electromagnetic solver for layered periodic structures". *Computer Physics Communications* 183 (10) (2012): pp. 2233–2244.

[35] M. Moharam and T. Gaylord. "Rigorous coupled-wave analysis of planar-grating diffraction". *JOSA* 71 (7) (1981): pp. 811–818.

[36] M. Moharam, E. B. Grann, D. A. Pommet, and T. Gaylord. "Formulation for stable and efficient implementation of the rigorous coupled-wave analysis of binary gratings". *JOSA a* 12 (5) (1995): pp. 1068–1076.

[37] M. Moharam, D. A. Pommet, E. B. Grann, and T. Gaylord. "Stable implementation of the rigorous coupled-wave analysis for surface-relief gratings: enhanced transmittance matrix approach". *JOSA A* 12 (5) (1995): pp. 1077–1086.

[38] M. Onishi, K. Crabtree, and R. A. Chipman. "Formulation of rigorous coupled-wave theory for gratings in bianisotropic media". *JOSA A* 28 (8) (2011): pp. 1747–1758.

[39] E. Popov and M. Nevière. "Grating theory: new equations in Fourier space leading to fast converging results for TM polarization". *JOSA A* 17 (10) (2000): pp. 1773–1784.

[40] E. Popov. "Gratings: theory and numeric applications". Popov, Institut Fresnel, 2012.

[41] E. Popov and M. Neviere. "Maxwell equations in Fourier space: fast-converging formulation for diffraction by arbitrary shaped, periodic, anisotropic media". *JOSA A* 18 (11) (2001): pp. 2886–2894.

[42] E. Popov, M. Nevière, B. Gralak, and G. Tayeb. "Staircase approximation validity for arbitrary-shaped gratings". *JOSA A* 19 (1) (2002): pp. 33–42.

[43] S Poulsen and P Bergander. *Gradient structure for transmitting and/or reflecting an electromagnetic signal*. Sweden Patent SE 544 804 C2, Nov. 2022.

[44] S. Rikte, G. Kristensson, and M. Andersson. "Propagation in bianisotropic media—reflection and transmission". *IEE Proc. Microwaves, Antennas and Propagation* 148 (1) (2001): pp. 29–36.

[45] K. Rokushima and J. Yamakita. "Analysis of anisotropic dielectric gratings". *JOSA* 73 (7) (1983): pp. 901–908.

[46] R. C. Rumpf. "Improved formulation of scattering matrices for semi-analytical methods that is consistent with convention". *Progress In Electromagnetics Research B* 35 (2011): pp. 241–261.

[47] T. Schuster, J. Ruoff, N. Kerwien, S. Rafler, and W. Osten. "Normal vector method for convergence improvement using the RCWA for crossed gratings". *JOSA A* 24 (9) (2007): pp. 2880–2890.

[48] D. Sjöberg, C. Engström, G. Kristensson, D. J. Wall, and N. Wellander. "A Floquet–Bloch decomposition of Maxwell's equations applied to homogenization". *Multiscale Modeling & Simulation* 4 (1) (2005): pp. 149–171.

[49] S. Spiridonov and A. A. Shcherbakov. "Reformulated Fourier modal method with improved near field computations". *Journal of Computational Science* 67 (2023): p. 101936.

[50] S. G. Tikhodeev, A. Yablonskii, E. Muljarov, N. A. Gippius, and T. Ishihara. "Quasiguided modes and optical properties of photonic crystal slabs". *Physical Review B* 66 (4) (2002): p. 045102.

[51] T. Vallius and M Honkanen. "Reformulation of the Fourier modal method with adaptive spatial resolution: application to multilevel profiles". *Optics Express* 10 (1) (2002): pp. 24–34.

[52] M. Van Beurden and I. Setija. "Local normal vector field formulation for periodic scattering problems formulated in the spectral domain". *JOSA A* 34 (2) (2017): pp. 224–233.

[53] Š. Višňovskỳ and K. Yasumoto. "Multilayer anisotropic bi-periodic diffraction gratings". *Czechoslovak Journal of Physics* 51 (2001): pp. 229–247.

[54] L. Wang, D. Fang, H. Jin, and J. Li. "2D rigorous coupled wave analysis with adaptive spatial resolution for a multilayer periodic structure". *Optics Express* 30 (12) (2022): pp. 21295–21308.

[55] L. Wang, D. Fang, H. Jin, and J. Li. "Global rigorous coupled wave analysis for design of multilayer metasurface absorbers". *Optics Express* 31 (24) (2023): pp. 40270–40284.

[56] T. Weiss, N. A. Gippius, S. G. Tikhodeev, G. Granet, and H. Giessen. "Derivation of plasmonic resonances in the Fourier modal method with adaptive spatial resolution and matched coordinates". *JOSA A* 28 (2) (2011): pp. 238–244.

[57] T. Weiss, G. Granet, N. A. Gippius, S. G. Tikhodeev, and H. Giessen. "Matched coordinates and adaptive spatial resolution in the Fourier modal method". *Optics express* 17 (10) (2009): pp. 8051–8061.

[58] D. Whittaker and I. Culshaw. "Scattering-matrix treatment of patterned multilayer photonic structures". *Physical Review B* 60 (4) (1999): p. 2610.

[59] W.-L. Yeh and Y.-P. Chiou. "A stable approach to conical diffraction of nearly lossless metallic gratings". *Optical and Quantum Electronics* 47 (2015): pp. 535–543.

[60] Z. Zhu and C. Zheng. "VarRCWA: an adaptive high-order rigorous coupled wave analysis method". *ACS photonics* 9 (10) (2022): pp. 3310–3317.